Bridge Deck Repair Investigation and Quantity Estimation

APPLIED RESEARCH &

INNOVATION BRANCH

Yail Jimmy Kim

COLORADO
Department of Transportation

Technical Report Documentation Page

1. Report No. CDOT-2020-19	2. Government Accession No.	3. Recipient's Catalog No.
4. Title and Subtitle Bridge Deck Repair Investigation and Quantity Estimation		5. Report Date Dec. 2020
		6. Performing Organization Code
7. Author(s) Yail Jimmy Kim		8. Performing Organization Report No.
9. Performing Organization Name and Address University of Colorado Denver 1200 Larimer St. Denver, CO 80217		10. Work Unit No. (TRAIS)
		11. Contract or Grant No. 217.03
12. Sponsoring Agency Name and Address Colorado Department of Transportation - Research 2829 W. Howard Pl. Denver CO, 80204		13. Type of Report and Period Covered Final
		14. Sponsoring Agency Code

15. Supplementary Notes

Prepared in cooperation with the US Department of Transportation, Federal Highway Administration

16. Abstract

This report presents a case study on the evaluation of bridge decks using various non-destructive test methods. In consultation with the Colorado Department of Transportation, five representative bridges are selected and assessed by qualitative/empirical (visual inspection and chain drag) and quantitative (ground-penetrating radar (GPR) and rebound hammer) approaches. The primary interest lies in quantifying delaminated areas in deck concrete covered with asphalt overlays. Analytical and computational models are formulated to decompose the intensity of GPR scales into two categories: i) initiation and progression of corrosion and ii) delamination of deck concrete, which show good agreement with repaired areas. Parametric investigations emphasize the significance of rebar spacing and concrete cover in determining the extent of deck delamination.

Implementation
- Current visual inspection methods employed at CDOT are adequate.
- The tolerable accuracy of GPR is ±20% at a 95% confidence interval.
- The severity of deterioration in GPR over 40% is taken for the estimation of deck delamination (40% to 100%).
- Rebound hammering is an alternative to GPR when a deck is not covered.
- The deteriorated area of deck concrete is inferred by adopting a threshold of 20% from the average strength measured by a rebound hammer

17. Keywords bridge decks; delamination; evaluation; ground-penetrating radar; non-destructive testing	18. Distribution Statement This document is available on CDOT's website https://www.codot.gov/programs/research		
19. Security Classif. (of this report) Unclassified	20. Security Classif. (of this page) Unclassified	21. No. of Pages	22. Price

Form DOT F 1700.7 (8-72)   Reproduction of completed page authorized

Acknowledgments

Executive Summary

This report presents a case study on the evaluation of bridge decks using various non-destructive test methods. In consultation with the Colorado Department of Transportation, five representative bridges are selected and assessed by qualitative/empirical (visual inspection and chain drag) and quantitative (ground-penetrating radar (GPR) and rebound hammer) approaches. The primary interest lies in quantifying delaminated areas in deck concrete covered with asphalt overlays, which has been a major problem in the bridge engineering community because conventional GPR contours provide a wide range of deterioration that differs from the amount of actual repair. A consistent condition rating of 7 has been assigned to all decks over a decade, aligning with the outcomes of chain drag: delamination of less than 3.31% of the entire deck area. The variable scanning frequencies of GPR (4 scans/ft to 20 scans/ft) influence contour mapping, whereas their statistical correlation is insignificant. A tolerable range of ±20% is suggested for interpreting GPR contour maps at a 95% confidence interval. The threshold limit of 20% used to identify degraded concrete in rebound hammering exhibits a coefficient of correlation of 0.967 against GPR-based deterioration; however, the results of these methods deviate from the areas of actual repair. For practical implementation, analytical and computational models are formulated to decompose the intensity of GPR scales into two categories: initiation and progression of corrosion (0% to 39%) and delamination of deck concrete (40% to 100%), which show good agreement with the repaired areas. Parametric investigations emphasize the significance of rebar spacing and concrete cover in determining the extent of deck delamination.

Implementation Statement

- Current visual inspection methods employed at CDOT are adequate.
- The tolerable accuracy of GPR is ±20% at a 95% confidence interval.
- The severity of deterioration in GPR over 40% is taken for the estimation of deck delamination (40% to 100%).
- Rebound hammering is an alternative to GPR when a deck is not covered.
- The deteriorated area of deck concrete is inferred by adopting a threshold of 20% from the average strength measured by a rebound hammer.

Keywords: bridge decks; delamination; evaluation; ground-penetrating radar; non-destructive testing

Table of Contents

List of Tables

List of Figures

1. Introduction

Infrastructure in the United States needs significant investment to accomplish safe, reliable, and resilient systems. The aging and deterioration of highway bridges are inevitable with time; thus, regular inspections and timely maintenance/repair enable the longevity of constituting elements. More than 5.4% of bridges in Colorado, carrying 2.5 million vehicles a day, were rated *structurally deficient* as of 2020, and the state is under consistent pressure from an insufficient budget of $136 million per year (ASCE 2020). Situations at the federal level are not different and the U.S. government planned a targeted budget of $300 million for the rehabilitation of bridges in poor condition (The White House 2019). As part of a structural system, bridge decks play an important role in transferring live load to super- and substructures, while the decks are vulnerable to deterioration because of direct exposure to detrimental distress such as vehicular loadings and deicing chemicals. Impaired decks should be repaired when delamination takes place, which is an intermediate stage in disintegration of the concrete between cracking and spalling. The occurrence of subsurface delamination is irregular and difficult to detect, so the amount can be approximated by theoretical and experimental investigations. Among the many sources responsible for delamination, corrosion along the reinforcing steel embedded in deck concrete is deemed to be salient; that is to say, the expansion of rust layers fractures the internal structure of the slab and abates its integrity (ElMaaddawy and Soudki 2007; ACI 2018). Chloride-induced delamination involves multiple processes consisting of electrochemical reactions for corrosion initiation and propagation, damage in the concrete-steel interface, and horizontal splitting (Wong et al. 2019; Meng et al. 2020).

It is imperative to adequately diagnose the condition of bridge decks before the formation of major faults, so that costly rehabilitation and replacement can be avoided. Non-destructive testing has been instrumental in detecting invisible defects without causing physical damage and addresses the limitations of conventional inspection methods (ACI 2013). Ground-penetrating radar (GPR) is an effective technique for the evaluation of bridge decks with overlays and is widely adopted. Gucunski et al. (2013) discussed the performance of GPR in terms of detecting deteriorated regions in existing decks. The principles, applications, and limitations of GPR technologies were explained with illustrative pictures. Recommendations include that GPR data,

representing probable deterioration, be used with other test results to better quantify on-site flaws. Hasan and Yazdani (2014) reported a case study on a bridge deck that was erroneously constructed with concrete covers shallower than those required by specifications. The as-built cover depth of the deck was measured using ground-coupled GPR, and more than 48 percent of the deck area possessed a cover depth of below 2.5 in. It was stated that concrete cover was important for GPR-scanning and coring benefitted site inspection results. Sultan and Washer (2018) examined the reliability of GPR and infrared thermography (IRT) concerning the delamination of bridge decks. Receiver operator characteristics (ROC) analysis was carried out to appraise the probability of false detection. In general, GPR generated a higher rate of false detection than IRT and overestimated delaminated areas; nonetheless, GPR still has merit since IRT cannot be used for asphalt-covered concrete decks. Rhee et al. (2020) studied the consequences of aging in overlaid decks with a focus on the dielectric properties of air-coupled GPR. Electromagnetic waves were monitored and analyzed to develop an empirical regression model, linking the age of concrete with GPR signals. Deteriorated decks showed a high dielectric constant owing to water-filled pores. A change in relative humidity by 10% up to 43 years precipitated an 11% increase in the dielectric constant.

Notwithstanding the popularity and usefulness, the outcomes of GPR are concerned with aggregated deterioration in asphalt-covered decks and do not provide appropriate information on concrete delamination, which is necessary for estimating the amount of repair. On account of such a drawback, bridge owners often encounter unexpected circumstances caused by differences between GPR-based planning and actual repair. For example, a rehabilitation project managed by the Colorado Department of Transportation had a GPR-surveyed repair quantity of 4,986 ft^2 in a covered deck; however, after removing the asphalt layer, actual areas were found to be 414 ft^2. The present case study aims to propose a refined GPR-interpretation approach extracting the quantity of concrete delamination from the deteriorated areas of deck slabs with asphalt overlays, which can facilitate a decision-making process for the maintenance and repair of highway bridges. Five benchmark reinforced concrete decks are singled out to investigate physical conditions through various nondestructive test methods (rebound hammer, chain drag, and GPR) as well as through the National Bridge Inventory (NBI) records associated with visual

inspections. Analytical and computational models are formulated and implemented to establish delamination criteria in the spatial domain of GPR.

2. Research Significance

Transportation agencies spend considerable efforts and resources to preserve the ride quality and structural integrity of bridge decks (Russell 2004). Unless major rehabilitation or replacement is carried out, the number of structurally deficient bridges does not decrease. Comprehensive inspections, followed by efficacious technical actions, are thus crucial to preclude the transition of bridge conditions from Excellent to Critical in the NBI scale (FHWA 2020). Delamination is a failure mode that increases life-cycle costs in reinforced concrete decks (Vu et al. 2005); as such, it needs to be properly gauged and handled. While many state DOTs publish inspection manuals for bridge decks, there is no mention about obtaining delaminated areas from GPR readings. This research deals with a systematic procedure to estimate the extent of delamination based on GPR contours.

3. Benchmark Bridges

Following the recommendations of the Colorado Department of Transportation, five bridges were selected (Fig. 1) and their configurations are enumerated in Table 1. These benchmark bridges encompassed a wide range of structural length from 22.2 ft to 272.5 ft, all of which had a skew angle of 10° to 55°. The design loads used were H20 (B06A), HS20 (C08A), and HS20+Mod or HS20 Interstate Alternate Loading (B06S, B06V, and C07A). Although the bridges have been in service for decades, there were no restrictions to daily traffic (Posting status = A). An increase in traffic was expected for the bridges, varying from 26% to 42% until 2031.
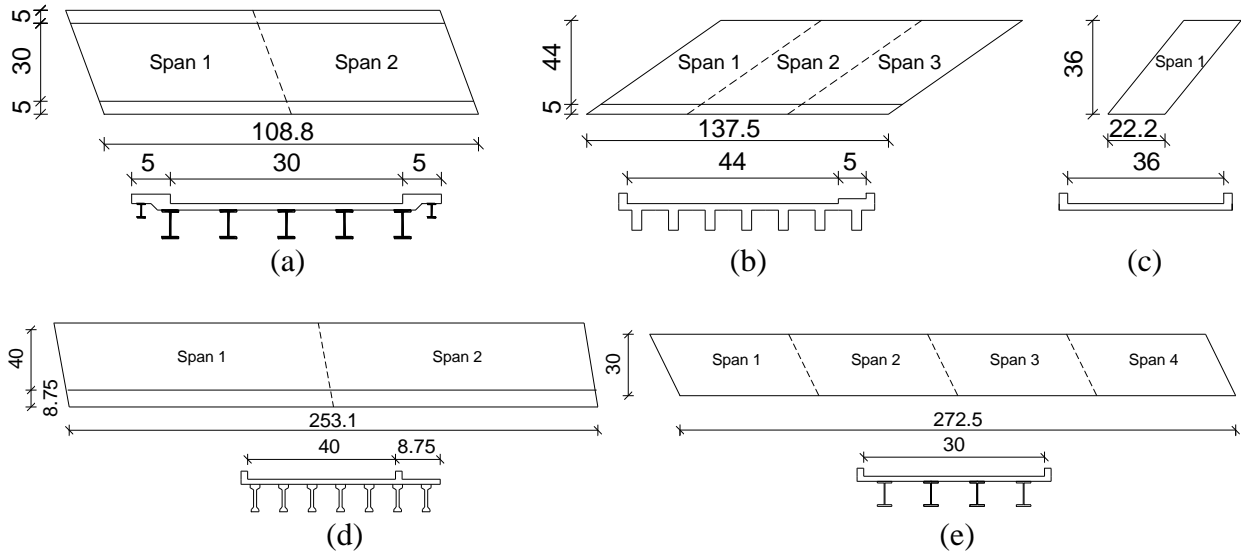
Fig. 1. Overview of benchmark bridges (units in ft): (a) B06A; (b) B06S; (c) C08A; (d) B06V; (e) C07A

Table 1. Nominal data of bridge structures

| ID | Year built | Number of spans | Length | Width | Skew | ADT | ADTT | Top steel rebar | | Asphalt overlay |
								Size	Spacing	Thickness
B06A	1952	2	108.8 ft	30 ft	30º	5,600	280	#5	12.75 in.	4.0 in.
B06S	1977	3	137.5 ft	44 ft	55º	3,000	330	#5	5.50 in.	3.0 in.
C08A	1954	1	22.2 ft	36 ft	40º	5,500	495	#4	9.00 in.	6.0 in.
B06V	1985	2	253.1 ft	40 ft	10º	3,200	192	#5	6.00 in.	1.3 in.
C07A	1967	4	272.5 ft	30 ft	30º	5,400	324	#5	10.00 in.	3.3 in.

ID = identification; Length = structural length; width = curb-to-curb width; ADT = average daily traffic; ADTT = average daily truck traffic; #4 = 0.5 in. diameter; #5 = 0.625 in. diameter

4. Nondestructive Testing

Various nondestructive test methods are employed to assess the quality of bridge decks, including qualitative/empirical (visual inspection and chain drag) and quantitative (ground-penetrating radar and rebound hammer) approaches. Because the decks are covered by overlays, chain-dragging and rebound-hammering are conducted when the asphalt layers are removed for an assessment and repair. A summary of on-site implementation is given below.

4.1. Visual Inspection

A qualified inspector performed technical evaluations to rate the structural and geometric conditions of the five bridges, which are subjected to an inspection frequency of 24 months for

updating the database of the NBI program. In spite of the simple and approximate nature, visual inspections offered convenient and rapid appraisals at low cost.

4.2. Ground-Penetrating Radar

As recognized in ASTM D6087 (ASTM 2008), GPR was the only available nondestructive test method for the examination of those asphalt-covered bridge decks. A contractor specializing in GPR technologies conducted field-scanning using ground-coupled antennas that were composed of a transmitter and a receiver. The GPR system was equipped with a set of dual 2-GHz antennas, positioned 15 in. above the deck surface (Fig. 2(a)). A device, called the electronic distance-measuring instrument, enabled continuous distance data. Electromagnetic waves were transmitted into the decks and reflections were recorded to quantify the severity of concrete degradation. Specifically, the signal attenuation and dielectric discontinuities of the reflected waves were interpreted to identify deteriorated regions, particularly for corrosion-induced damage in the top mat of reinforcing steel and subsequent concrete delamination (the primary causation of such delamination is the expansion of corrosion rust surrounding the reinforcement, Scott et al. 2003; Yehia et al. 2007). In addition, the depth of the rebars and the thickness of the overlays were measured.
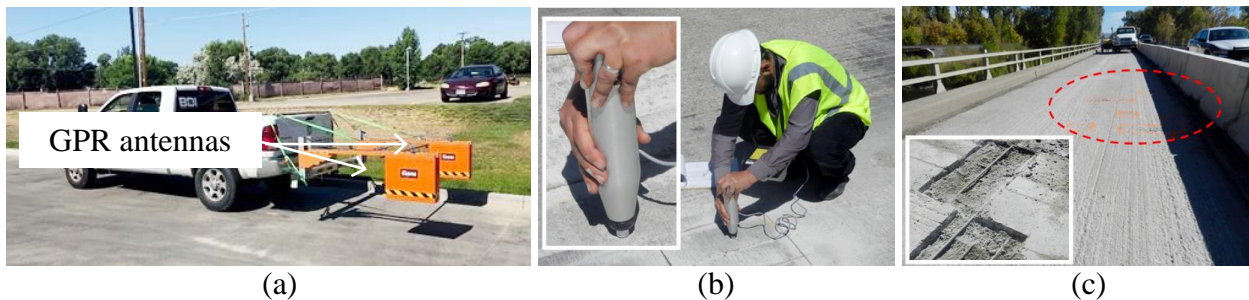

(a)   (b)   (c)

Fig. 2. Nondestructive tests: (a) air-coupled ground-penetrating radar; (b) rebound hammer; (c) marked areas and exposed rebars for repair after chain dragging

The transverse spacing between GPR readings was less than 3 ft, leading to approximately ten lines per bridge deck, and the range of ambient temperature was between 88°F and 93°F without precipitation. To study the scanning sensitivity of the air-coupled GPR, variable sampling rates were tested from 4 scans/ft to 20 scans/ft in the longitudinal direction. Traffic control was not

necessary during the acquisition of GPR data. Graphics software generated two-dimensional contour maps to visually assess the deterioration of the individual decks.

4.3. Rebound Hammer

With reference to ASTM C805 (ASTM 2018), a rebound hammer test was carried out. Each traffic lane of the bridges was divided into three to four lines, and the strength of the deck concrete was recorded at intervals of 7 ft, as pictured in Fig. 2(b). Since rebound readings are concerned with the hardness of an elastic material (Teodoru 1988), degradation of the concrete cover (deck surface to top bars) was of interest. While performing rebound hammering, care was exercised to avoid direct contact with exposed aggregates, leading to false-strength data. It should be noted that data for C08A were not available due to unexpected difficulties in the field.

4.4. Chain Drag

Chain drag was performed as guided by ASTM D4580 (ASTM 2012) to determine the quantities of repair. Even if this method is empirical and cannot detect local delaminations, it is broadly used owing to convenience. An experienced field engineer dragged steel chains on the deck surface, compared tonal differences (clear vs. dull), and marked possible delaminated regions. Afterward, the designated areas were saw-cut and the deck concrete was in part replaced (Fig. 2(c)).

5. Test Results

Per non-destructive test results, the deterioration level of the five benchmark bridge decks is discussed. Logged data are analyzed quantitatively and characterized statistically.

5.1. Visual Inspection

Table 2 provides the evaluative information of the bridge decks excerpted from the NBI for the last decade (2010 to 2019). The deck condition rating was maintained to be 7 (*Good condition*: some minor problems); consequently, no major maintenance and rehabilitation were necessary. The geometric classifications of the decks, concerning width and vertical clearance, were generally related to year-built. For example, C08A and B06V, constructed in 1954 and 1985,

respectively, received ratings of 4 and 6, respectively. A widening project was scheduled for B06A, built in 1952 and rated 3.

Table 2. Information from the National Bridge Inventory (NBI) from 2010 to 2019

Identification	Deck condition	Deck geometry evaluation
B06A	7	3
B06S	7	9
C08A	7	4
B06V	7	6
C07A	7	4

5.2. Ground-Penetrating Radar

5.2.1. Interpretation of scanned data

The cross-sectional images of pristine and deteriorated deck regions are displayed in Figs. 3(a) and (b), respectively, where the representative views of B06A are given for brevity and other bridges showed similar GPR results. The magnitudes of the bounced wave signals depended upon electrical conductivity and relative dielectric permittivity (Gucunski et al. 2013), which produced visually distinguishable layer structures in the deck. The attenuated signals in the deteriorated regions (Fig. 3(b)), resulting from dissipated electromagnetic energy (Benedetto and Benedetto 2011), signify the presence of chlorides, cracking, and delamination in the deck concrete (Gucunski et al. 2013). Since electromagnetic waves were not able to penetrate the steel reinforcement (Giannopoulos et al. 2002), the top-bar location was conspicuous. Likewise, the interface between the asphalt and concrete was detected via their difference in dielectric contrast. Table 3 enumerates the depth of the top steel and overlays measured from the deck surface. Due to cracking, wearing, and abrasion (Figs. 3(c) and (d)), the actual overlay thickness varying from 1.7 in. to 2.6 in. was shallower than the nominal thickness shown in Table 1 (1.3 in. to 6.0 in.). The net depth of the reinforcement was between 2.1 in. and 3.2 in. at an average coefficient of variation (COV) of 0.141 without the overlays, which was reasonably close to the concrete cover of 2.5 in. specified in the American Association of State Highway Transportation Officials (AASHTO) Load and Resistance Factor Design (LRFD) Bridge Design Specifications (AASHTO 2017).
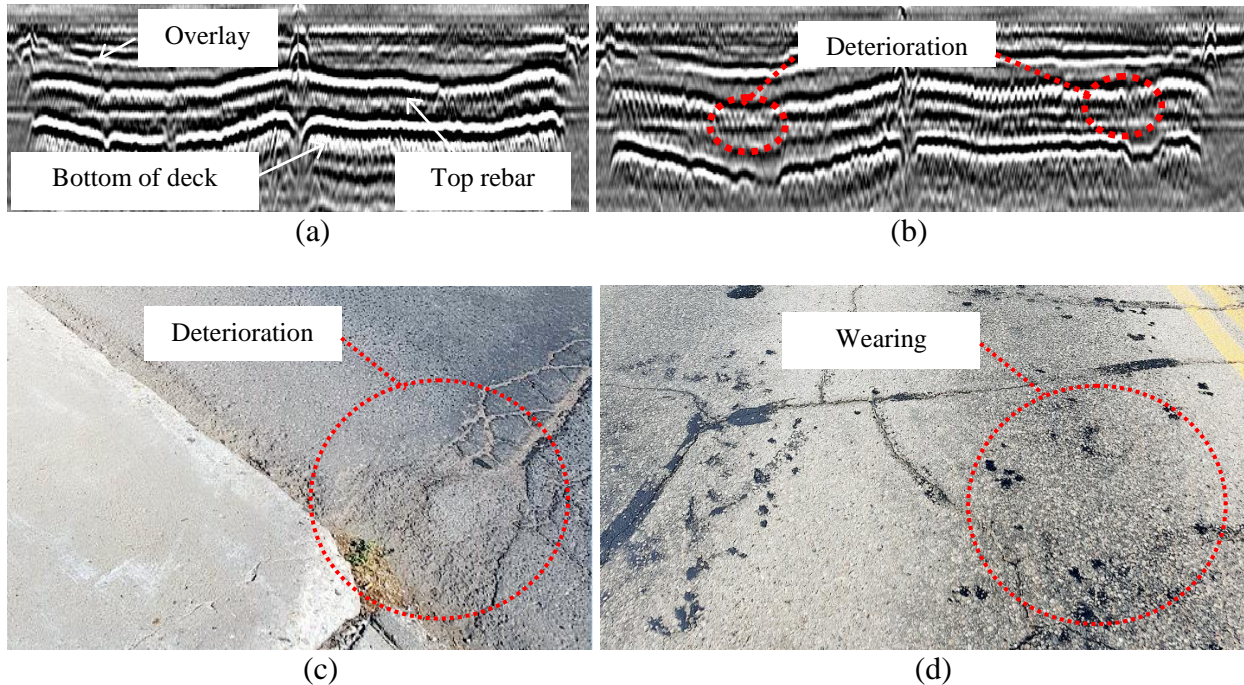
Fig. 3. Scanned images of ground-penetrating radar and conditions of overlays: (a) pristine section (B06A); (b) deteriorated section (B06A); (c) deterioration of overlay (B06A); (d) wearing of overlay (B06V)

5.2.2. Effect of scanning frequency

The severity of deterioration used for the assessment of the GPR data is defined in Fig. 4(a), which aligns with the weakened electromagnetic signals (Fig. 3). The scale bar was developed with decibel thresholds, based on ASTM D6087 (ASTM 2008) and experts' refined mesh; however, details are not reported due to the proprietary claim of the contractor. Figures 4(b) to (f) plot the deteriorated regions of B06S at variable scanning frequencies. Although the GPR data generated analogous images, the areas of deterioration varied from 659 ft^2 to 847 ft^2, as summarized in Table 3. This illustrates that the GPR readings were influenced by the scanning frequency and that the amplitude of the signal reflection was not a deterministic quantity, supported by other GPR analyses (Shin and Grivas 2003). Furthermore, as reported in literature (Hing and Halabe 2010), the accuracy of GPR is another notable factor affecting the quantification of deteriorated areas since its minimal detectable ability is limited to 4 in.^{2}.

Table 3. Ground penetrating radar data

Bridge ID	Total area[1] (ft^2)	Scan rate (scan/ft)	Deterioration			Average rebar depth[2] (in.)	Average overlay thickness[2] (in.)
			Area (ft^2)	Ratio (%)	Average (%)		
B06A	3,264	4	414	12.7	12.6	5.2	2.0
		8	402	12.3			
		12	416	12.7			
		16	387	11.9			
		20	440	13.5			
B06S	6,050	4	659	10.9	12.1	5.1	2.6
		8	847	14.0			
		12	773	12.8			
		16	672	11.1			
		20	719	11.9			
C08A	799	4	75	9.4	7.6	4.9	2.6
		8	57	7.1			
		12	55	6.9			
		16	70	8.8			
		20	45	5.6			
B06V	10,124	4	1,311	12.9	12.7	4.5	1.7
		8	1,174	11.6			
		12	1,300	12.8			
		16	1,243	12.3			
		20	1,402	13.8			
C07A	8,175	4	1,698	20.8	21.4	4.1	2.0
		8	1,874	22.9			
		12	1,650	20.2			
		16	1,818	22.2			
		20	1,722	21.1			

[1] Total area = structural length (NBI Item No. 49) multiplied by curb-to-curb width (NBI Item No. 51)

[2] Measured from deck surface

(a)　　　　　　(b)　　　　　　(c)

(d)　　　　　　(e)　　　　　　(f)
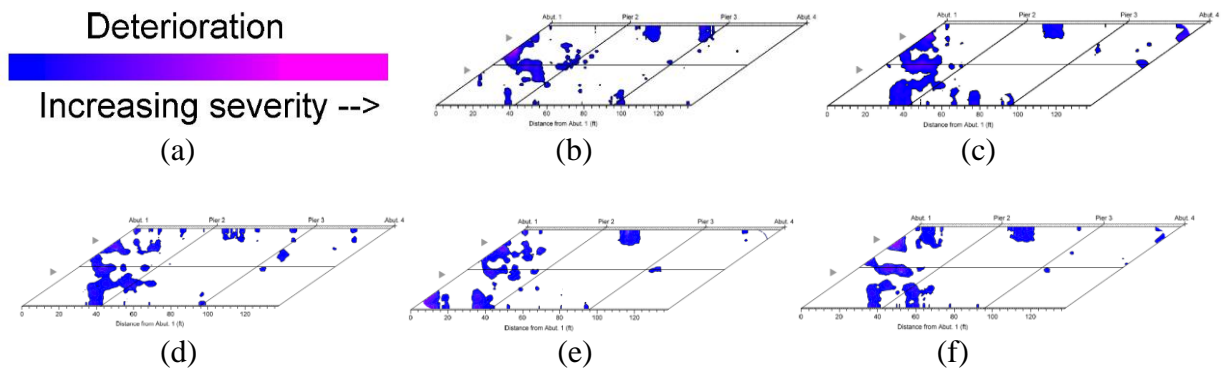
Fig. 4. Variable data collection rates on deck of B06S: (a) deterioration scale of ground-penetrating radar; (b) 4 scans/ft; (c) 8 scans/ft; (d) 12 scans/ft; (e) 16 scans/ft; (f) 20 scans/ft

5.2.3. Layout of deteriorated decks

Figure 5 shows the GPR maps of the five decks. For the convenience of a visual assessment, the severity scale was not present and the maps obtained from the respective scanning frequencies were combined. As quantified in Table 3, the average deterioration of C08A was the least (7.6% of the total deck area) and the deterioration of B06A, B06S, and B06V was similar (12.6%, 12.1%, and 12.7% of the total deck areas, respectively). On the contrary, relatively large areas were detected in the case of C07A along all spans (21.4% of the total deck area). Provided that patching is typically conducted if deterioration is less than 30% of a deck area (Hema et al. 2004), these bridges were repaired accordingly (to be discussed in a later section).
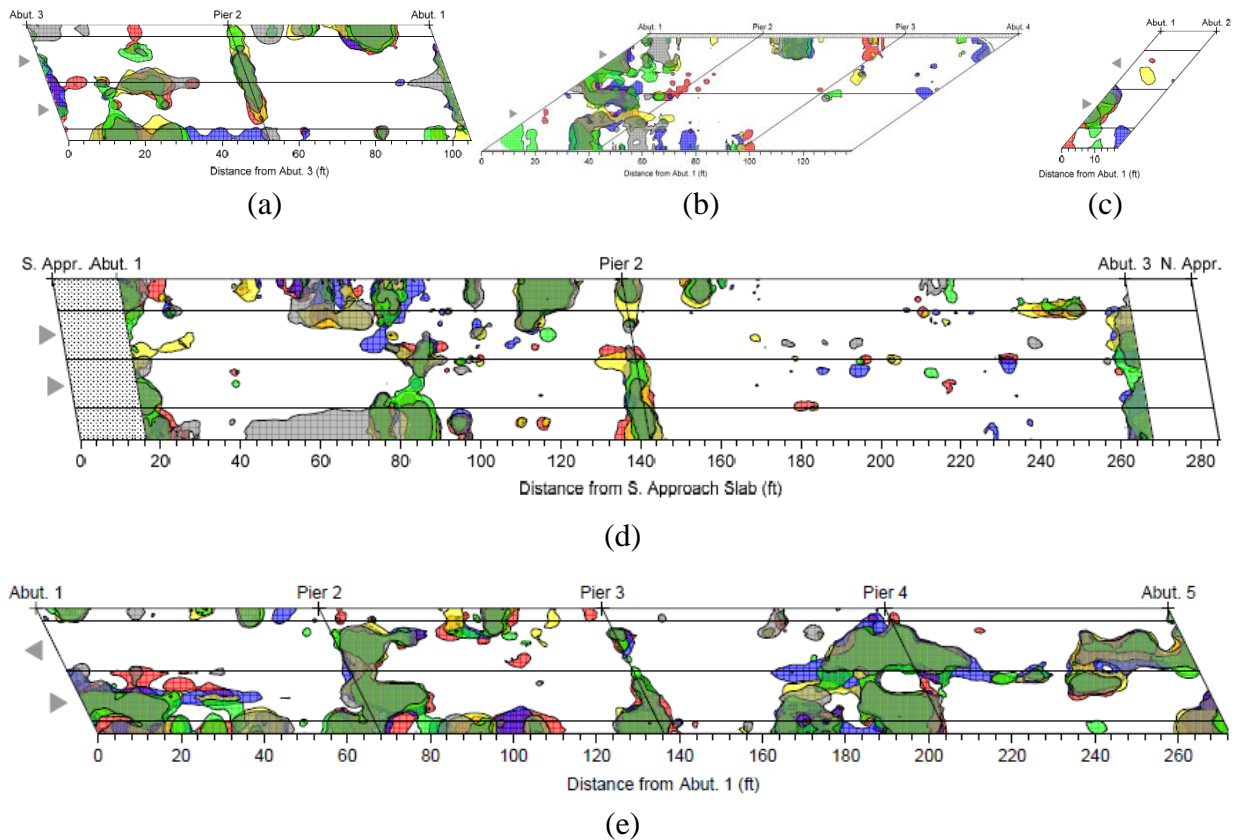
Fig. 5. Scanned bridge decks by ground-penetrating radar: (a) B06A; (b) B06S; (c) C08A; (d) B06V; (e) C07A

5.2.4. Sensitivity analysis

The percent deterioration of the decks with the scan rate is graphed in Fig. 6(a). There was no correlation between the scanning frequency and the deteriorated area. Considering the COV

values positioned between 0.047 and 0.203 (Fig. 6(b)), the degree of scatter in the GPR readings appeared reasonable. It is noted that the standard GPR test for bridge decks (ASTM D6087 (ASTM 2008)) does not state an acceptable range of accuracy; hence, further research is recommended. As an alternative for evaluating the sensitivity of the measured GPR data, confidence intervals were calculated at a level of 95% (Meeker et al. 2017)

$$\mu - 1.96 \frac{\sigma}{\sqrt{n}} \leq \mu \leq \mu + 1.96 \frac{\sigma}{\sqrt{n}} \tag{1}$$

where μ and σ are the mean and standard deviation of the data, respectively, and n is the number of GPR repetitions per bridge. The confidence intervals of the decks were normalized by their means for comparison and are given in Fig. 6(c). The lower and upper levels of C08A (0.82 and 1.18, respectively) enveloped all other cases, meaning that ±20% of the GPR data can be tolerable within the 95% confidence intervals. Figure 6(d) exhibits the results of factorial analysis, which clarifies the statistical significance of the GPR properties. An F_0 statistic is calculated (Montgomery 2013) and compared against the corresponding threshold limit (a confidence level of 95% was used for consistency, $F_{0.05}$): if F_0 is greater than $F_{0.05}$, the factor is regarded to be significant; otherwise, insignificant. The value of $F_0 = 49.41$ in the bridge type factor ($> F_{0.05} = 3.63$) attests that the GPR readings were dominated by the bridge configurations; on the other hand, the scanning rate was not a significant factor ($F_0 = 0.07 < F_{0.05} = 3.63$). The interaction between these two factors (bridge type and scanning rate) was not significant either ($F_0 = 0.38 < F_{0.05} = 5.12$). That is, the GPR-based deterioration was bridge-specific and the scanning rate was not a critical factor from a statistical perspective.
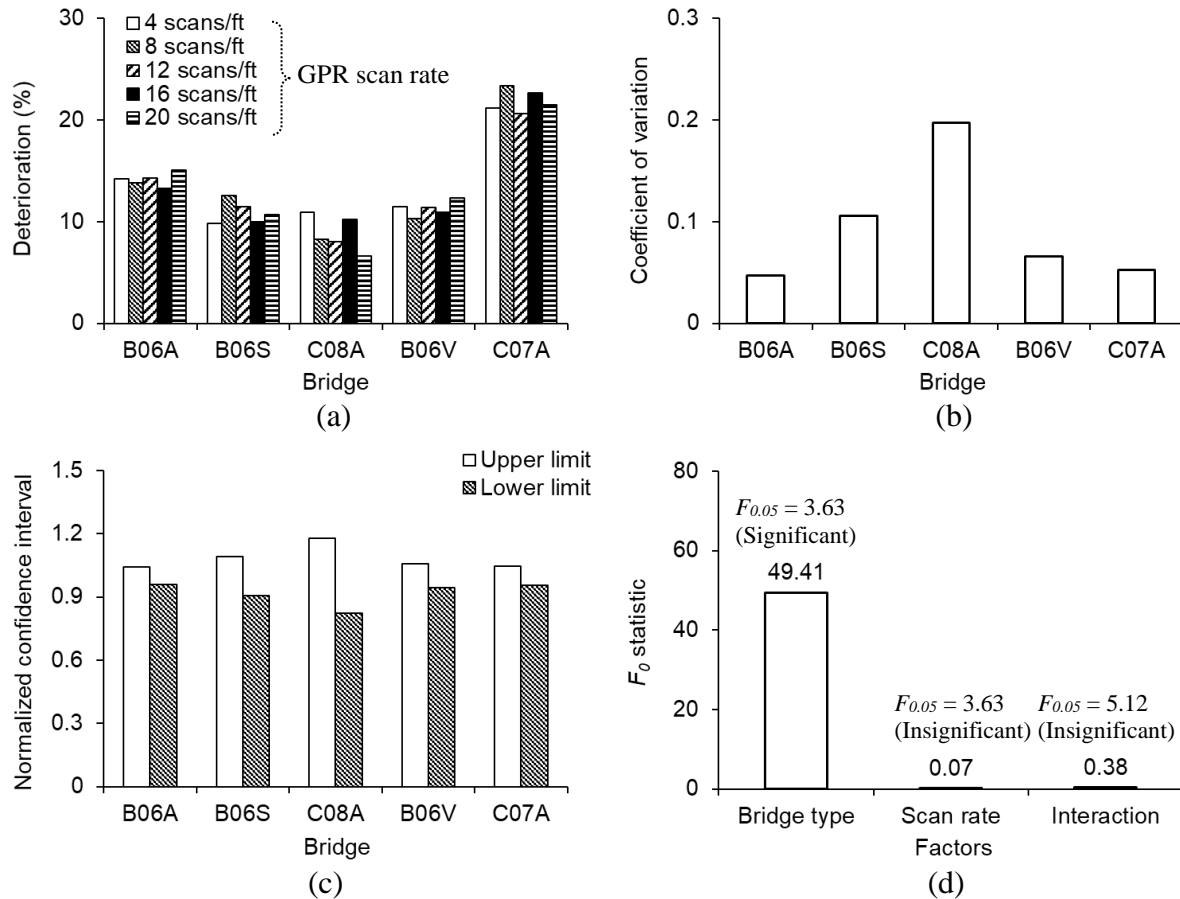
Fig. 6. Sensitivity analysis of ground-penetrating radar: (a) scanned data for deterioration; (b) coefficient of variation; (c) confidence interval; (d) factorial analysis

5.3. Rebound Hammer

Figure 7 shows the compressive strength of the deck concrete. For the purpose of comparison, the strength and span length of the individual bridges were normalized by corresponding average strength and total span, respectively. The line numbers indicated in Figs. 7(a) to (d) represent the repeated strength measurements along the decks, contingent upon superstructure size and accessibility at the time of rebound hammering. The strength variation of the deck concrete was acceptable, as supported by the coefficient of variation ranging from COV = 0.061 to 0.131: an archetypal COV for structural concrete is 0.125 (Nowak and Collins 2013). Conforming to the published literature that defines a degradation threshold for hardened concrete (Elmenshawi and Brown 2010; Khoshraftar et al. 2013; Guo et al. 2014), a 20% reduction of the average strength was set as the limit. The percentage of the measured values below the threshold was then multiplied by the deck area of each bridge to estimate the quantity of deterioration. As shown in

Fig. 8(a), a linear trend was noticed between the deteriorated areas determined from the GPR and rebound hammering, and the coefficient of correlation (Eq. 2) was $P_{cor} = 0.967$ (1.0 = perfect correlation)

$$P_{cor} = \frac{\sum_{i=1}^{n_c}(x_i - x_m)(y_i - y_m)}{\sqrt{\sum_{i=1}^{n_c}(x_i - x_m)^2}\sqrt{\sum_{i=1}^{n_c}(y_i - y_m)^2}} \tag{2}$$

where n_c is the sample size; and x_i and y_i are the individual abscissa (rebound hammer) and ordinate (GPR), respectively, and their means are x_m and y_m, respectively. This fact implies that, if a deck is not covered with overlays, rebound hammering can be a cost-saving option for conjecturing the area of deterioration.
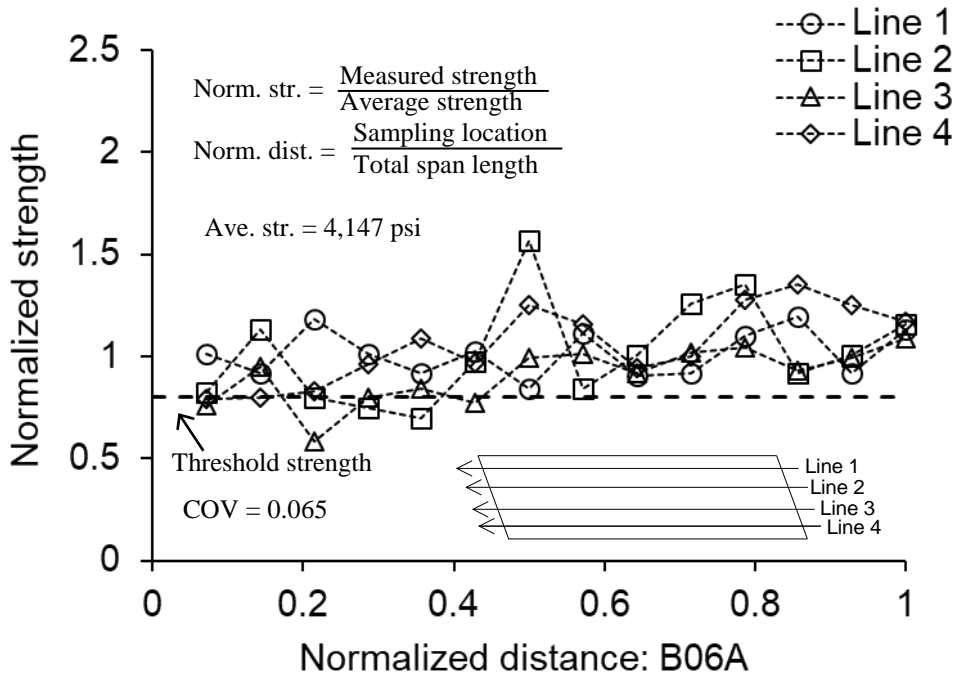
(a)
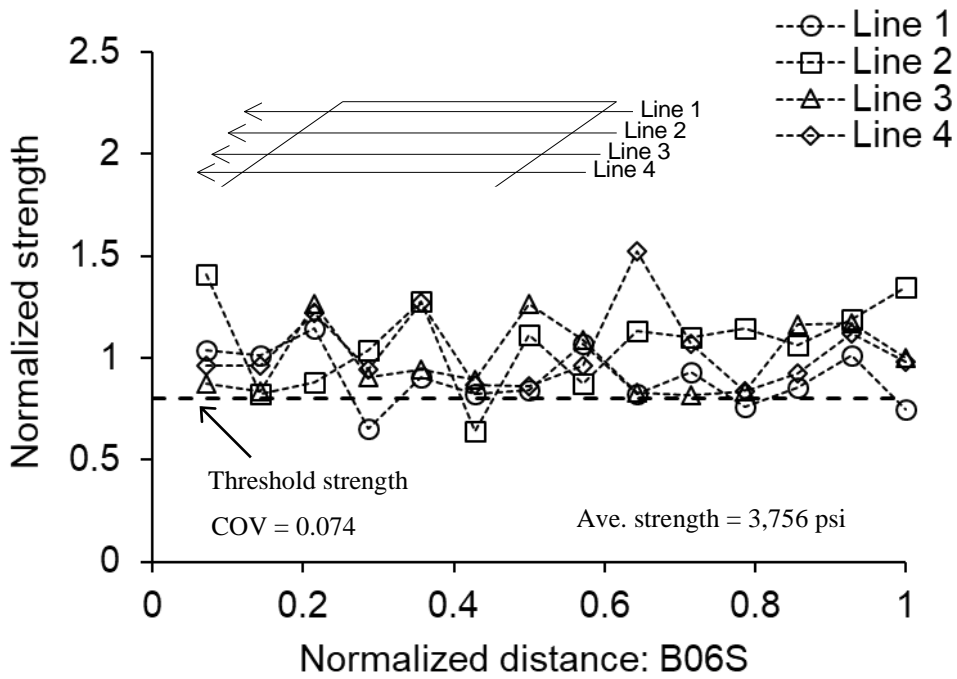
(b)

Fig. 7. Rebound hammer data: (a) B06A; (b) B06S

14
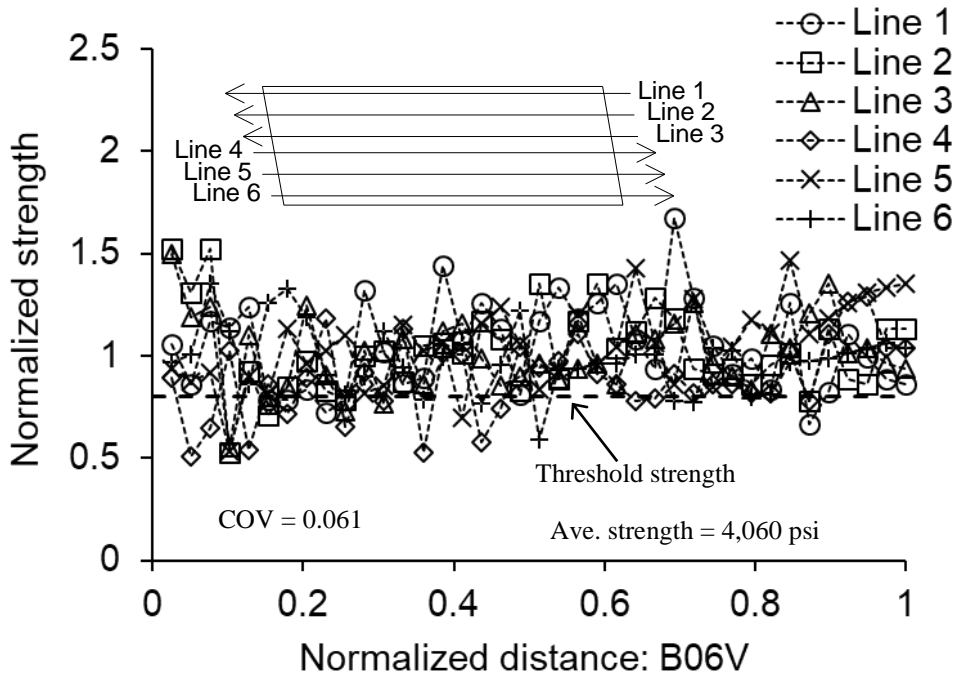
(c)
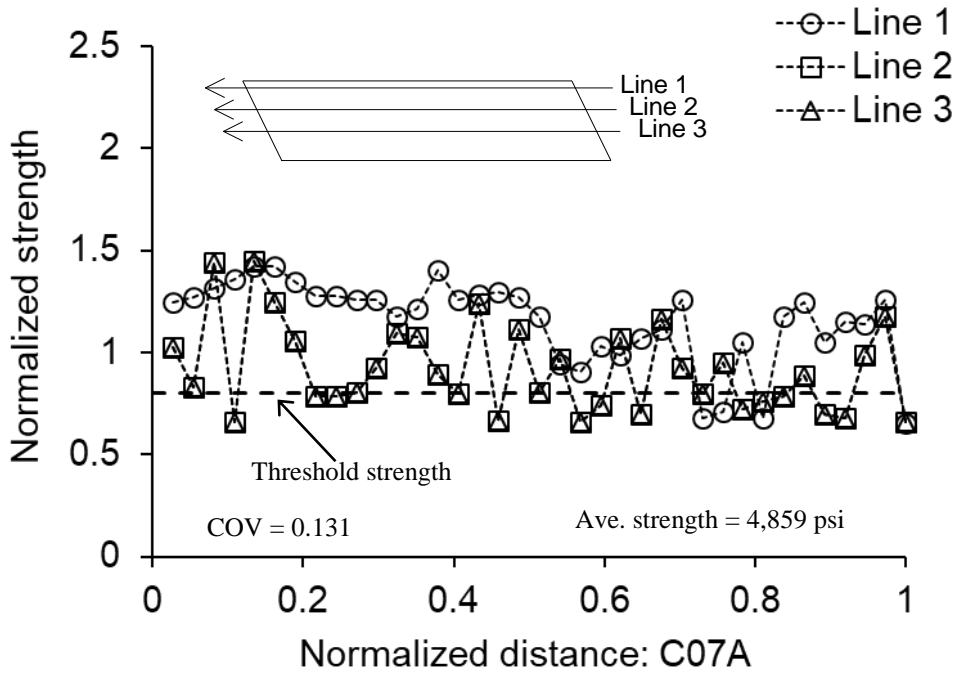
(d)

Fig. 7. Rebound hammer data: (c) B06V; (d) C07A

5.4. Chain Drag and Repair

According to the results of chain drag, the decks were repaired (Table 4). The patched area of C07A was the largest (270.8 ft^2 (25.2 m^2)), whereas those of B06A and C08A were none. The amounts of actual repair (0% to 3.31% of the deck areas) denote that the condition of the bridge decks was close to a rating of 7 in the conventional scale of the Federal Highway Administration (delamination < 2% of deck area, FHWA 1979) and reaffirm the adequacy of the NBI records delineated in Table 2. The repaired areas, however, differed from the deteriorated areas previously quantified by the GPR and rebound hammering (Fig. 8(b)). To demonstrate the extent of mutual agreement between the test methods, the significance factor (I) proposed by Barnes and Trottier (2004) was modified ($I \geq 5$ means a noticeable discrepancy)

$$I = \frac{\left(A_A - A_B\right)^2}{A_{deck}} \tag{3}$$

Table 4. Comparison of actual repair with deteriorated and delaminated deck areas

Bridge ID	Actual repair		Scan rate (scan/ft)	GPR deterioration		Model-based delamination					
	Area (ft^2)	Ratio (%)		Average area (ft^2)	Ratio (%)	Exact			Low bound		
						Area (ft^2)	Average (ft^2)	Ratio (%)	Area (ft^2)	Average (ft^2)	Ratio (%)
B06A	0	0	4	412	12.6	18.44	9.15	0.28	26.96	13.03	0.39
			8			7.59			9.25		
			12			15.35			19.98		
			16			4.17			7.06		
			20			0.22			1.92		
B06S	20.9	0.35	4	734	12.1	0	0	0	7.67	7.85	0.13
			8			0			2.94		
			12			0			0.74		
			16			0			15.03		
			20			0			12.87		
C08A	0	0	4	60	7.5	14.77	3.21	0.40	17.59	4.34	0.54
			8			0			0.54		
			12			0			0.00		
			16			0			0.75		
			20			1.29			2.83		
B06V	7.6	0.08	4	1,286	12.7	0	0.25	0.00	34.40	45.78	0.45
			8			0.89			49.11		
			12			0.34			44.13		
			16			0			31.44		
			20			0.03			69.80		
C07A	270.8	3.31	4	1,752	21.4	161.46	99.12	1.21	161.46	99.12	1.21
			8			112.91			112.91		
			12			88.6			88.6		
			16			42.28			42.28		
			20			90.34			90.34		

Ratio = ratio to total deck area

where A_A and A_B are the areas detected by methods A and B (either chain drag vs. rebound hammer or chain drag vs. GPR in this section), respectively, and A_{deck} is the total deck area. As shown in Fig. 8(b), all factors were classified into the *highly significant* ($I > 15$) and *moderately significant* ($5 < I < 15$) categories. This necessitates isolating concrete delamination from the deteriorated regions.

[1 ft^2 = 0.093 m^2]
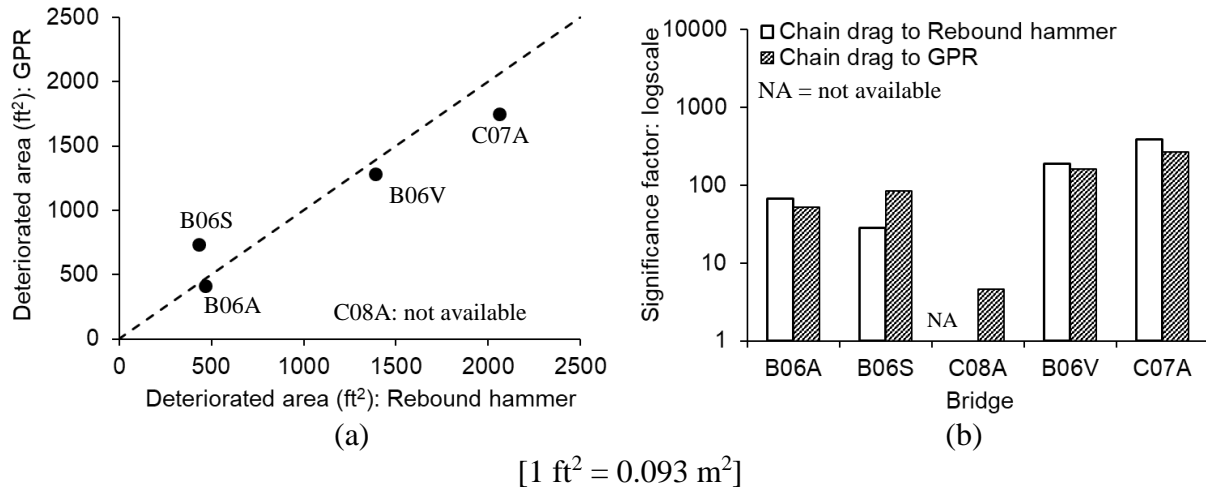
Fig. 8. Evaluation of rebound hammer results: (a) average deterioration; (b) significance factor

6. Assessment of Delamination

Since repairs are conducted when concrete delamination occurs, delaminated areas need to be extracted from a GPR map that represents deteriorated concrete. Figure 9(a) depicts a schematic diagram concerning the progressive degradation of a corrosion-damaged bridge deck. In accordance with analytical modeling and computational simulations, the regions of delaminated concrete are predicted and compared against repaired areas.

17
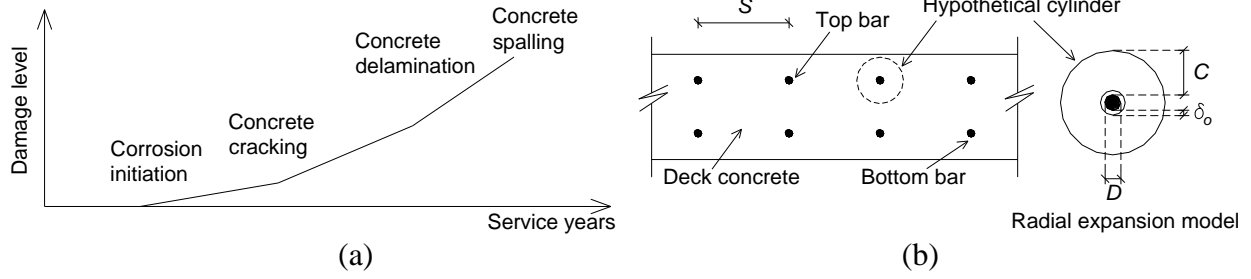
Fig. 9. Deterioration of bridge deck: (a) progression of damage; (b) analytical model

6.1. Formulation

6.1.1. Analytical modeling

As illustrated in Fig. 9(b), the radial expansion of deck concrete due to rebar corrosion, δ, may be obtained by (ElMaaddawy and Soudki 2007)

$$\delta = \frac{(1+\upsilon+\psi)(D+2\delta_0)}{2E_{eff}} P \tag{4}$$

$$\psi = \frac{(D+2\delta_0)^2}{2C(C+D+2\delta_0)} \tag{5}$$

where P is the radial pressure induced by the formation of corrosion rust; υ is the Poisson's ratio of concrete ($\upsilon = 0.2$); D is the diameter of the intact steel reinforcement; δ_0 is the thickness of the porous zone between the concrete and reinforcement ($\delta_0 = 0.0008$ in. (20 μm), Thoft-Christensen 2000); C is the thickness of the hypothetical cylinder wall (C = clear cover of the rebar); and E_{eff} is the effective elastic modulus of the concrete, which is defined as (ACI 2008; ACI 2019)

$$E_{eff}(t) = \frac{E_c(0)}{1+\phi(t)} \tag{6}$$

$$E_c(0) = 57,000\sqrt{f_c'} \text{ in psi} \tag{7a}$$

$$E_c(0) = 4,730\sqrt{f_c'} \text{ in MPa} \tag{7b}$$

$$\phi(t) = \frac{(t-t_0)^{0.6}}{10+(t-t_0)^{0.6}} \phi_u \tag{8}$$

where $E_c(0)$ and f'_c are the initial elastic modulus and compressive strength of the concrete, respectively; $\phi(t)$ is the creep coefficient at time t in days; t_0 is the initial time when the concrete

18

is loaded ($t_0 = 28$ days was assumed); and ϕ_u is the ultimate creep coefficient ($\phi_u = 2.35$). The corrosion initiation time (t_i) in years is determined using (Thoft-Christensen et al. 1996)

$$t_i = \frac{(C/10)^2}{4D_{ce}}\left(erf^{-1}\left(\frac{C_{cr}-C_0}{C_i-C_0}\right)\right)^{-2}$$ (9)

where D_{ce} is the diffusion coefficient in cm^2/s ($D_{ce} = 3.1 \times 10^{-9}$ in.^{2}/s (2.0×10^{-8} cm^2/s) for a typical deck, Stewart and Rosowsky 1998); erf is the Gauss error function; C_{cr} and C_i are the critical and initial chloride concentrations ($C_{cr} = 0.4\%$ and $C_i = 0\%$ of the cement weight, Elsener and Angst 2016); and C_0 is the equilibrium chloride ($C_0 = 1.6\%$, Thoft-Christensen et al. 1996). The concrete cracks when the radial pressure reaches the tensile strength (ElMaaddawy and Soudki 2007; ACI 2019)

$$P_{cr} = \frac{2Cf_r}{D}$$ (10)

$$f_r = 7.5\sqrt{f_c'} \quad \text{in psi}$$ (11a)

$$f_r = 0.62\sqrt{f_c'} \quad \text{in MPa}$$ (11b)

where P_{cr} is the radial pressure at cracking and f_r is the modulus of rupture. Combining Eqs. 4 and 10 yields the concrete expansion at cracking (δ_{cr})

$$\delta_{cr} = \frac{(1+\upsilon+\psi)(D+2\delta_0)Cf_r}{DE_{eff}}$$ (12)

With the assumption that energy losses due to cracking are negligible and the corrosion products are uniform around the rebar, the rust-induced expansion can continue until the deck concrete delaminated at (Bazant 1979; Cady and Weyers 1984)

$$\delta_{del} = \frac{f_r}{2}\left(\frac{S}{D}-1\right)\delta_{pp} \geq \delta_{cr}$$ (13)

$$\delta_{pp} = \left(\frac{D(1+\phi(t))}{E(0)}\right)\left(1+\upsilon+D^2\left(\frac{2}{S^2}+\frac{1}{4C(C+D)}\right)\right)$$ (14)

where δ_{del} is the concrete expansion at delamination and S is the spacing of the rebars.

6.1.2. Agent-based modeling

Preprocessing: The deterioration of the GPR contours was decoded in RGB model space, comprising a combination of Red, Green, and Blue, so that the condition of the bridge decks was numerically linked with the scale bar (Fig. 10(a), inset). The intensities of these colors varied from 0 to 255; for instance, a value set of (255, 0, 0) means red. After completing a calibration process (Fig. 10(a)), the GPR maps of the individual decks were imported to a two-dimensional space in the Netlogo platform. This computer program is specialized in simulating the decentralized response of a discrete agent, called *patch*, that is controlled by a preset rule. The principle and applications of Netlog are provided elsewhere (Wilensky 1999). The dimensions of the imported images were defined and a grid system was assigned to envelop each deck. In doing so, the number of image pixels became equal to the number of the patches; accordingly, one agent represented one pixel with a specific color in the RGB space.
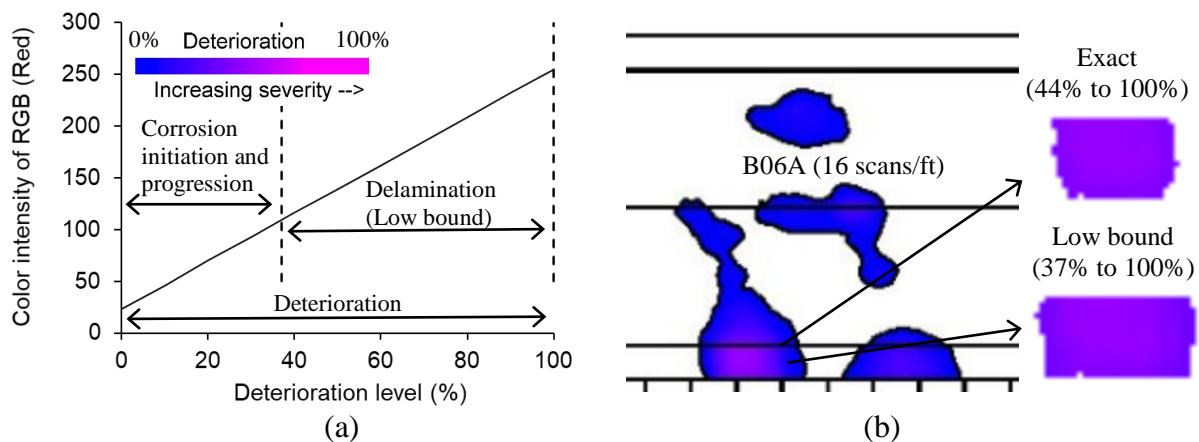
Fig. 10. Agent-based modeling: (a) calibration of RGB color code; (b) extracted delaminated areas at exact and low bound levels for B06A

Implementation: The delaminated areas of the decks were obtained by two categories: the Exact level was used as calculated from the model, while the Low bound level was intended for practical application. The Exact level included a color range spanning from a certain λ value to λ = 100% belonging to the respective decks, where λ is the delamination ratio between cracking and delamination to be determined using the aforementioned analytical model ($\lambda = \delta_{cr}/\delta_{cr}$ in Eqs. 12 and 13); by contrast, the Low bound level contained the low delamination ratio of the five decks (Fig. 10(a), details are given in the subsequent section). The discrete patches of the decks

20

recognized individual pixel colors, and the intensities of Red were attained in the RGB space to identify the calibrated deterioration levels (Fig. 10(b)). Then, the number of the patches was counted within a designated color range and multiplied by a single pixel size to determine the delaminated areas of the decks.

6.2. Delamination of Deck Concrete

6.2.1. Model-based delamination

Figure 11(a) exhibits the corrosion initiation years of the bridge decks, based on the cover depth of the reinforcement measured by GPR (Table 3). The corrosion of B06A commenced at 13.2 years, while that of C07A began at 5.7 years. These predicted results are conservative because the asphalt overlays listed in Table 3 were not taken into consideration in the empirical model. A comparison between the radial expansions at the cracking and delamination (δ_{cr} and δ_{del}, respectively) of B06S is provided in Fig. 11(b), along with the average concrete strength determined by the rebound hammer tests (Fig. 7). After the onset of corrosion at 8.1 years, the radial expansions marginally increased and the gap between the cracking and delamination was maintained up to 100 years. It is important to note that the deck concrete was not subjected to cracking and delamination as soon as the rebar corrosion initiated, whereas the predictions in Fig. 11(b) indicate possible expansion patterns over time (the ratio between these expansions is the above-defined delamination ratio, λ). Compared with the concrete expansion at cracking, additional rust-induced pressures were required for delamination, as given in the skewed data in Fig. 11(c): the strength of C08A was not measured so it was assumed to be the average of the other four bridges' strengths. The difference between the cracking and delamination was a function of the bridge configuration (Fig. 11(d)), and the δ_{cr}/δ_{del} ratios ranged from 37% to 100%. This observation points out that the delamination of the concrete deck can be approximated above 37% of the deterioration intensity in the GPR scale (Fig. 4(a)). In other words, 0% to 36% of the GPR scale represents the initiation of corrosion and progression (Fig. 10(a)); for that reason, the chain drag did not detect the concrete damage within this range (human ear can only perceive an audible range of 1 to 3 kHz, Gucunski et al. 2013) and thus the repair work was not available.
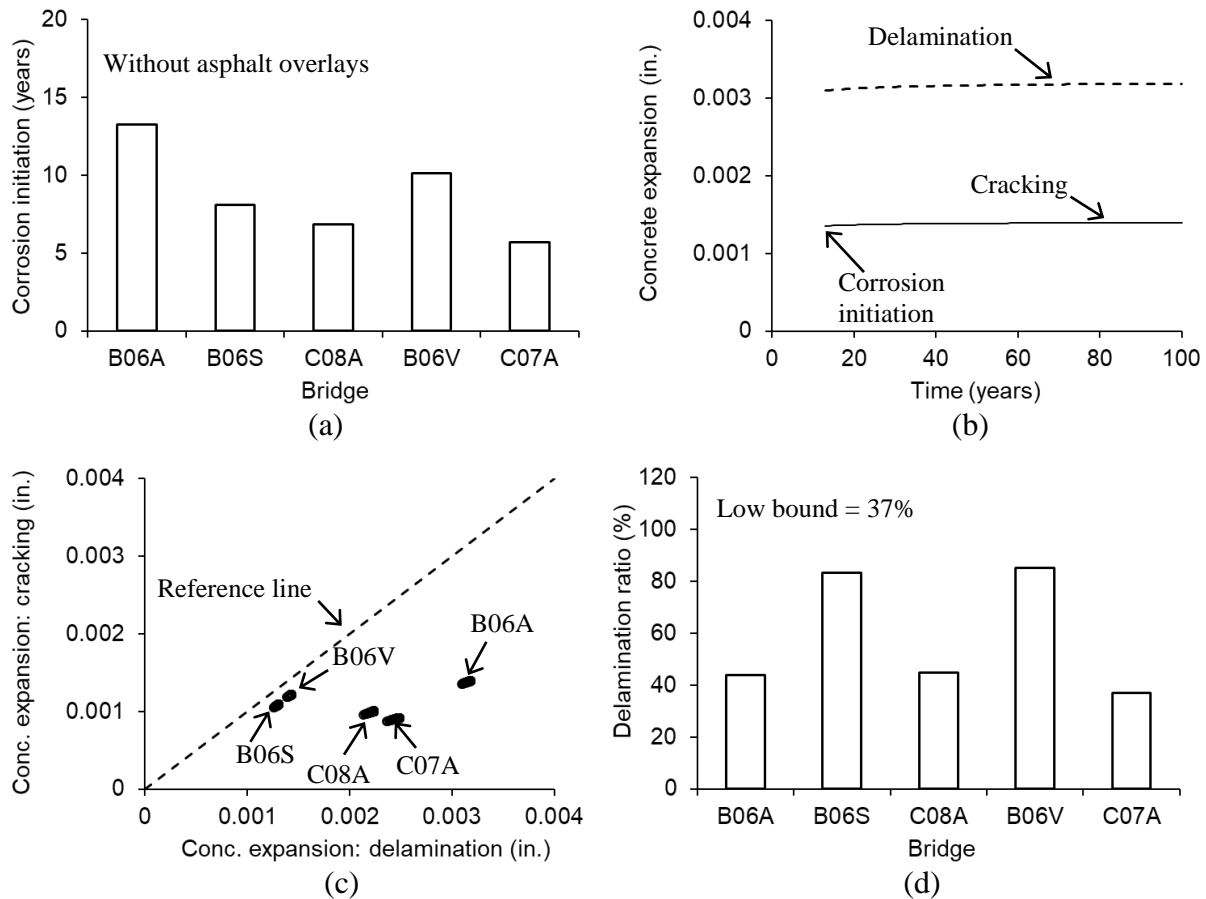
Fig. 11. Corrosion-induced damage: (a) corrosion initiation time; (b) concrete expansion due to corrosion at cracking and delamination for B06A; (c) comparison among bridges; (d) average delamination ratio for 100 years

6.2.2. Evaluation

A comprehensive evaluation of the GPR and model-based delamination is shown in Fig. 12. The average responses of the models with the Exact and Low bound levels were comparable (Fig. 12(a)), although their scan-rate-dependent values fluctuated due to the inconsistency of the GPR contours (Table 4). As evidenced in Fig. 12(b), the normalized deck areas associated with GPR were substantially larger than those with the models. There were minor discrepancies between the Exact and Low bound results (Fig. 12(b), inset); therefore, the Low bound model covering all the five bridges (Fig. 11(d)) was adopted for the estimation of the delaminated areas. The degree of deviation from the actual repair is clearly discernable in the Model and GPR (Figs. 12(c) and (d)). From an application standpoint, the dissimilarity between the Model and actual repair is

22

negligible because the accuracy of chain drag is affected by numerous factors with a large COV of 40% (Scott et al. 2003; Maser 2004).
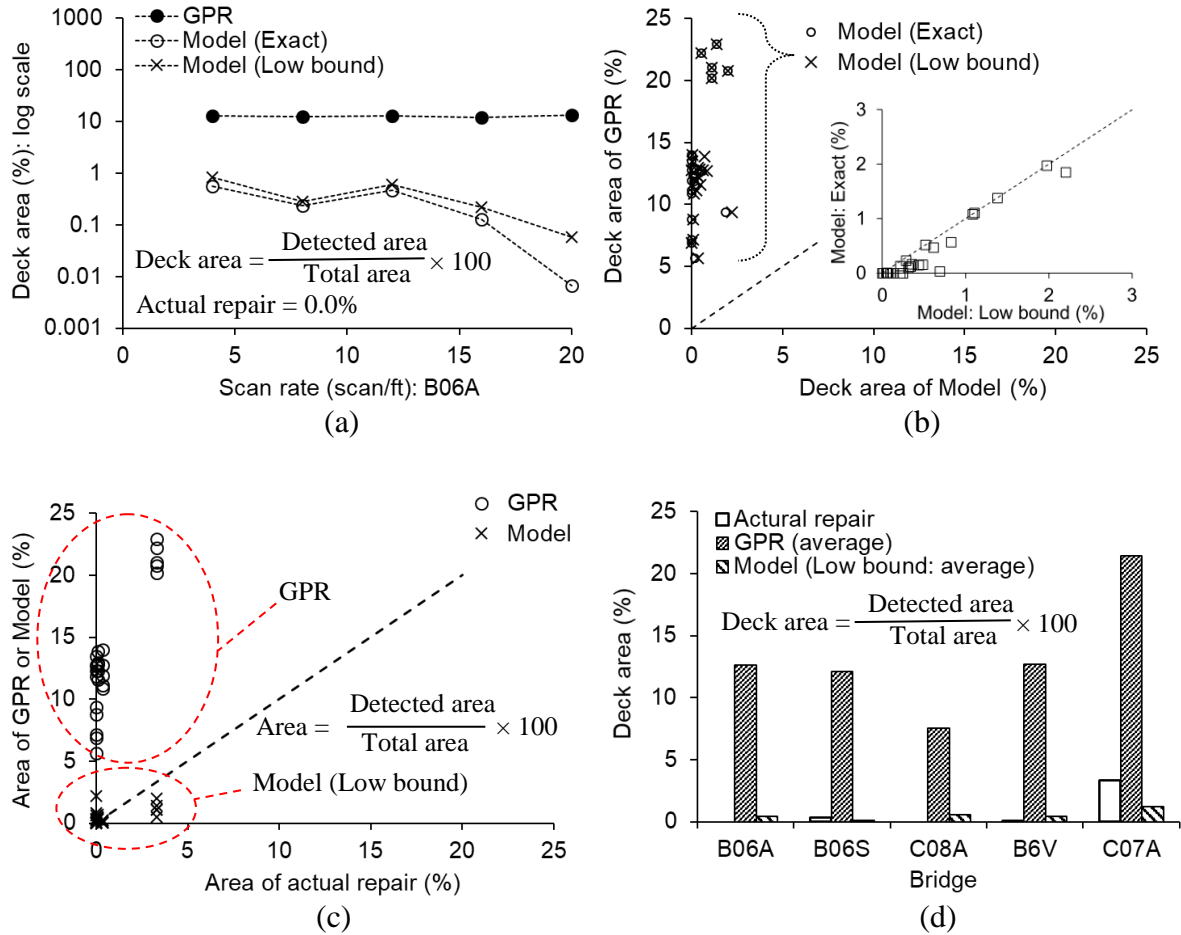
Fig. 12. Evaluation of delaminated area: (a) deck area with scan rate for B06A; (b) comparison between GPR and model; (c) comparison among actual repair, GPR, and model; (d) average comparison

6.2.3. Parametric study

The sensitivity of constituent parameters in the analytical model is described in Fig. 13. The default properties for the chloride-induced corrosion were taken as presented earlier (Eq. 9), and those for the delamination ratio (λ) were as follows (values for all other variables in Eqs. 12 to 14 remained unchanged): compressive strength of concrete = 4,000 psi (27 MPa), diameter and spacing of No. 5 rebar = 0.625 in. (15.9 mm) and 8 in. (203 mm), respectively, and service period = 100 years. The corrosion initiation year (t_i) linearly decreased with the increased critical chloride concentration (C_{cr}, Fig. 13(a)); in contrast, the year gradually rose when the equilibrium

23

chloride (C_o, Fig. 13(b)) went up. Despite the difficulty in accurately inferring the onset of corrosion, the practical range of the C_{cr} and C_0 terms implies that bridge decks under ordinary circumstances begin to corrode between 5 and 10 years, which is corroborated by previous studies (Hopper et al. 2015; Li 2019). Unlike the concrete strength (3,000 psi (20 MPa) to 5,000 psi (35 MPa)) and rebar diameter (0.25 in. (6.35 mm) to 0.625 in. (15.9 mm), No. 3 to No. 5) showing insignificant effects on the delamination ratio of the deck (Figs. 13(c) and (d)), the concrete cover for the top rebars (2.5 in. (64 mm) to 4.0 in. (102 mm)) and rebar spacing (4 in. (102 mm) to 10 in. (254 mm)) were dominant parameters that altered the delamination ratio (Figs. 13 (e) and (f)). Within the simulation ranges of these parameters, the resultant delamination ratios were above the ratio of 37% at the Low bound level (Fig. 11(d)). Thereby, a rounded ratio of 40% is suggested when interpreting GPR data for delamination of concrete decks; namely, the scale bar of a GPR map can be decomposed into the initiation and progression of corrosion (0% to 39%), accompanied by concrete cracking, and the delamination of the concrete (40% to 100%).
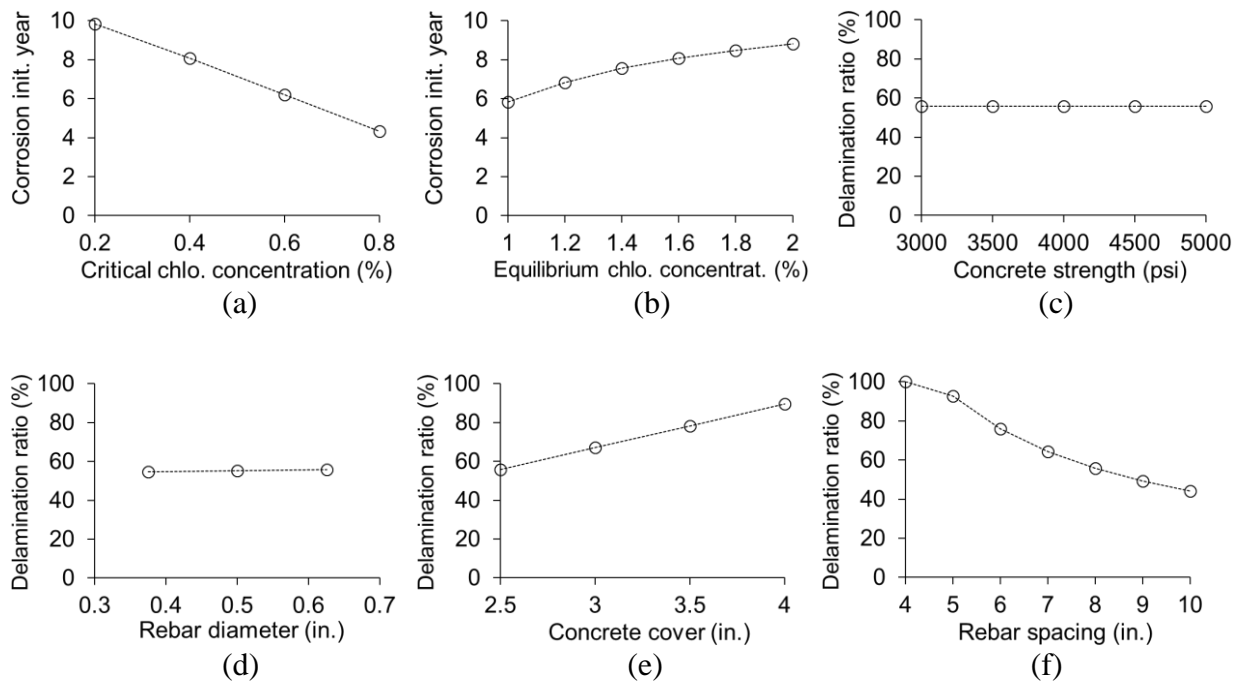
Fig. 13. Parametric study: (a) critical chloride concentration; (b) surface chloride concentration; (c) concrete strength; (d) rebar diameter; (e) concrete cover; (f) rebar spacing

6.2.4. Independent appraisal

The reproducibility of the proposed method is shown in Figs. 14(a) and (b). These bridges (N-10-V and I-12-T) are located in Colorado, and GPR-scanning was conducted to graphically examine the condition of the decks. The agent-based model effectively replicated the most deteriorated regions, indicated in red. The delamination ratio of $\lambda = 40\%$ was, then, applied to the GPR map of another bridge (F-20-BQ) on the interstate highway I-70 (Fig. 14(c)). The bridge was constructed in 1966 with a roadway width of 39.5 ft (12 m) and a length of 140 ft (43 m), including the total deck area of 5,530 ft^2 (514 m^2). An NBI deck rating of 4 was assigned at the time of GPR-testing in 2014 and the patch-repaired area was 1,067 ft^2 (99 m^2). The area of deterioration (delamination) was quantified to be 2,898 ft^2 (269 m^2) and 498 ft^2 (46 m^2) by GPR and infrared spectroscopy, respectively. In compliance with the proposed modeling approach, a delaminated area of 1,022 ft^2 (95 m^2) was acquired at $\lambda = 40\%$ (Fig. 14(c), inset), which revealed an improved result against the repaired area.
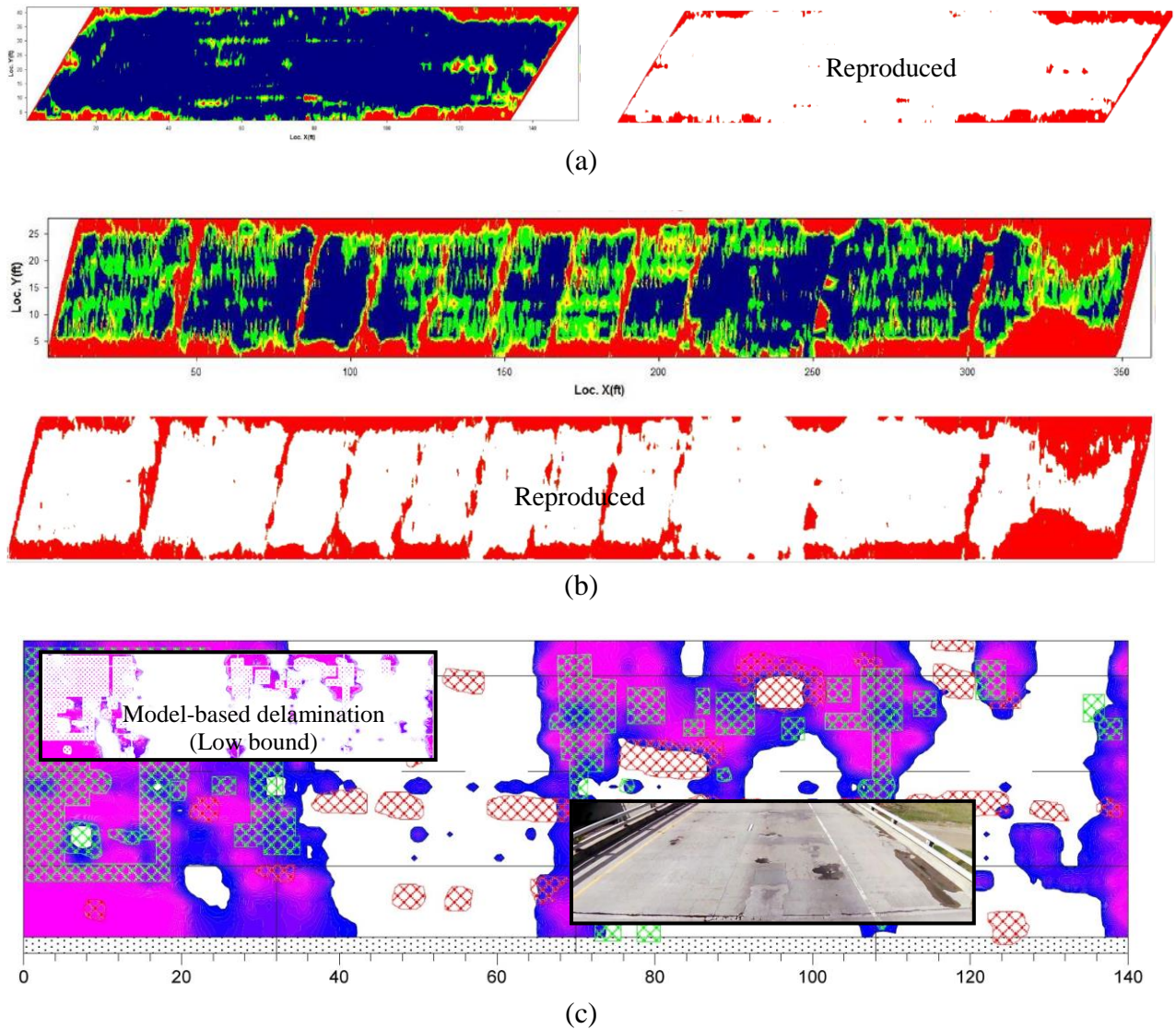
Fig. 14. Independent appraisal of proposed approach: (a) reproducibility of GPR maps (Bridge N-10-V); (b) reproducibility of GPR maps (Bridge I-12-T); (c) Bridge F-20-BQ for (green grids = patched area; red grids = damage detected by infrared spectroscopy)

7. Summary and Conclusions

The effectiveness of various non-destructive test methods has been investigated through five existing bridges in Colorado. Emphasis was placed on quantifying delaminated areas in asphalt-overlaid deck concrete. Both qualitative/empirical (visual inspection and chain drag) and quantitative (GPR and rebound hammer) approaches were tested and their data were analyzed comparatively. The GPR contour maps at variable scanning frequencies were employed to assess the extent of deterioration, and further integrated with analytical models for figuring out

26

delaminated concrete areas under two decoding levels: Exact and Low bound. The adequacy of patch repair was elaborated in tandem with chain drag. The following are conclusions from the present case study

- Aligning with chain drag in terms of a delaminated area ratio, which was less than 3.31% of the entire deck area, the visual inspection provided a consistent deck rating of 7 (*Good condition*: some minor problems) for a ten-year period.

- The deterioration of the decks enveloped a broad range from the initiation of rebar corrosion to the delamination of concrete. Even though the scanning frequencies affected GPR readings, their statistical correlation was insignificant. The suggested tolerable range of ±20% in GPR can be considered when interpreting contour maps at a 95% confidence interval.

- On the rebound hammering, the degree of scatter was noticed between COV = 0.061 and 0.131 for measuring the strength of the deck concrete. The degradation threshold of 20% provided comparable results against the GPR-based deterioration with a coefficient of correlation of 0.967. As per the calculated significance factors, the repaired areas of the decks deviated from the deteriorated areas determined by the GPR and rebound hammer.

- The time for corrosion initiation was conservatively predicted from 5.7 to 13.2 years in the decks. The Low bound level of the model extracted delaminated areas using the deterioration intensity of the GPR scale above 40%, and good agreement was made with the repaired areas. The applicability of the proposed model was independently confirmed by three additional bridges. Parametric investigations clarified that the influence of rebar spacing and concrete cover was noteworthy for evaluating the delaminated areas.

8. Implementation of Research

For the practical implementation of research findings, the following recommendations are provided:

- Current visual inspection methods employed at CDOT are adequate.
- The tolerable accuracy of GPR is ±20% at a 95% confidence interval.

- Taking the severity of deterioration in GPR over 40% generates a reasonable amount of deck delamination (40% to 100%). If a repair is planned solely relying on GPR contour maps (0% to 100%), there may be a large discrepancy between estimation and actual repair.

- Rebound hammering is an alternative to GPR when a deck is not covered. The deteriorated area of deck concrete is inferred by adopting a threshold of 20% from the average strength measured in the field.

9. References

AASHTO. 2017. AASHTO LRFD bridge design specifications (8th edition), American Association of State Highway Transportation Officials, Washington, D.C.

ACI. 2008. Guide for modeling and calculating shrinkage and creep in hardened concrete (ACI 209.2R-08), American Concrete Institute, Farmington Hills, MI.

ACI. 2013. Report on nondestructive test methods for evaluation of concrete in structures (ACI 228.2R-13), American Concrete Institute, Farmington Hills, MI.

ACI. 2018. Concrete terminology (ACI CT-18), American Concrete Institute, Farmington Hills, MI.

ACI. 2019. Building code requirements for structural concrete and commentary (ACI 318-19), American Concrete Institute, Farmington Hills, MI.

ASCE. 2020. Infrastructure report card, American Society of Civil Engineers, Reston, VA.

ASTM. 2008. Standard test method for evaluating asphalt-covered concrete bridge decks using ground penetrating radar (ASTM D6087-08), ASTM International, West Conshohocken, PA.

ASTM. 2012. Standard practice for measuring delaminations in concrete bridge decks by sounding (ASTM D4580-12), ASTM International, West Conshohocken, PA.

ASTM. 2018. Standard test method for rebound number of hardened concrete (ASTM C805-18), ASTM International, West Conshohocken, PA.

Barnes, C.L. and Trottier, J.-F. 2004. Effectiveness of ground penetrating radar in predicting deck repair quantities, Journal of Infrastructure Systems, 10(2), 69-76.

Bazant, Z.P. 1979. Physical model for steel corrosion in concrete sea structures, Proceedings, ASCE, 105(ST6), 1137-1167.

Benedetto, A. and Benedetto, F. 2011. Remote sensing of soil moisture content by GPR signal processing in the frequency domain, Sensors Journal, 11(10), 2432-2441.

Cady, P.D. and Weyers, R.E. 1984. Deterioration rates of concrete bridge decks, Journal of Transportation Engineering, 110(1), 34-44.

ElMaaddawy, T. and Soudki, K. 2007. A model for prediction of time from corrosion initiation to corrosion cracking, Cement and Concrete Composites, 29, 168-175.

Elmenshawi, A. and Brown, T. 2010. Hysteretic energy and damping capacity of flexural elements constructed with different concrete strengths, Engineering Structures, 32, 297-305.

Elsener, B. and Angst, U. 2016. Corrosion inhibitors for reinforced concrete, Science and Technology of Concrete Admixtures, 321-339.

FHWA. 1979. Recording and coding guide for structure inventory and appraisal of the nation's bridges, Federal Highway Administration, Washington, D.C.

FHWA. 2020. National bridge inventory, Federal Highway Administration, Washington, D.C.

Khoshraftar, A., Abbasnia, R., and Raof, F.F. 2013. The effect of degradation on seismic damage of RC buildings, Advances in Environmental Biology, 7(5), 861-867.

Giannopoulos, A., Macintyre, P., Ridgers, S., and Forde, M.C. 2002. GPR detection of voids in post-tensioned concrete bridge beams, Proceedings of SPIE, 4758, 376-381.

Gucunski, N., Imani, A., Romero, F., Nazarian, S., Yuan, D., Wiggenhauser, H., Shokouhi, P., Taffe, A., and Kutrubes, D. 2013. Nondestructive testing to identify concrete bridge deck deterioration, SHRP 2 Report S2-R06A-RR-1, Transportation Research Board, Washington, D.C.

Guo, Y.-C., Zhang, J.-H., Chen, G.-M., and Xie, Z.-H. 2014. Compressive behaviour of concrete structures incorporating recycled concrete aggregates, rubber crumb and reinforced with steel fibre, subjected to elevated temperatures, Journal of Cleaner Production, 72, 193-203.

Hasan, M.I. and Yazdani, N. 2014. Ground penetrating radar utilization in exploring inadequate concrete covers in a new bridge deck, Case Studies in Construction Materials, 1, 104-114.

Hema, J., Fonseca, F.S., Guthrie, W.S. 2004. Concrete bridge deck condition assessment and improvement strategies, Report No. UT-04-16, Utah Department of Transportation, Taylorsville, UT.

Hing, C.L.C. and Halabe, U.B. 2010. Nondestructive testing of GFRP bridge decks using ground penetrating radar and infrared thermography, Journal of Bridge Engineering, 15(4), 391-398.

Hopper, T., Manafpour, A., Radinska, A., Warn, G., Rajabipour, F., Morian, D., and Jahangirnejad, S. 2015. Bridge deck cracking: effects on in-service performance, prevention, and remediation, Final Report No. FHWA-PA-2015-006-120103, Pennsylvania Department of Transportation, Harrisburg, PA.

Li, V.C. 2019. Engineered cementitious composites: bendable concrete for sustainable and resilience infrastructure, Springer, Berlin, Germany.

Maser, K. 2004. Active heating infrared thermography for detection of subsurface bridge deck deterioration, Final Report for Highway IDEA Project 101, Transportation Research Board, Washington, D.C.

Meeker, W.Q., Hahn, G.J., and Escobar, L.A. 2017. Statistical intervals: a guide for practitioners and researchers (second edition), John Wiley and Sons, Hoboken, NJ.

Meng, D., Lin, S., and Azari, H. 2020. Nondestructive corrosion evaluation of reinforced concrete bridge decks with overlays: an experimental study, Journal of Testing and Evaluation 48(1), 516-537.

Montgomery, D.C. 2013. Design and analysis of experiments (eighth edition), John Wiley and Sons, Hoboken, NJ.

Nowak, A.S. and Collins, K.R. 2013. Reliability of structures (second edition), CRC Press, Boca Raton, FL.

Rhee, J.-Y., Park, K.-E., Lee, K-.H., and Kee, S.-H. 2020. A practical approach to condition assessment of asphalt-covered concrete bridge decks on Korean Expressways by dielectric constant measurements using air-coupled GPR, Sensors, 20, 2497.

Russell, H.G. 2004. Concrete bridge deck performance (NCHRP Synthesis 333), Transportation Research Board, Washington, D.C.

Scott, M., Rezaizadeh, A., Delahaza, A., Santos, C.G., Moore, M., Graybeal, B., and Washer, G. 2003. A comparison of nondestructive evaluation methods for bridge deck assessment, NDT&E International, 36, 245-255.

Shin, H. and Grivas, D.A. 2003. How accurate is ground-penetrating radar for bridge deck condition assessment?, Journal of the Transportation Research Board, 1845(1), 139-147.

Stewart, M.G. and Rosowsky, D.V. 1998. Time-dependent reliability of deteriorating reinforced concrete bridge decks, Structural Safety, 20(1), 91-109.

Sultan, A.A. and Washer, G.A. 2018. Comparison of two nondestructive evaluation technologies for the condition assessment of bridge decks, Transportation Research Record, 2672(41), 113-122.

The White House. 2019. Deliver 21st century infrastructure, The Executive Office of the President of the United States, Washington, D.C.

Teodoru, G. 1988. The use of simultaneous non-destructive tests to predict the compressive strength of concrete, Nondestructive Testing, ACI-SP-112, American Concrete Institute, Farmington Hills, MI.

Thoft-Christensen, P. 2000. Stochastic modelling of the crack initiation time for reinforced concrete structures, Structural Congress, American Society of Civil Engineers, 8 pp.

Thoft-Christensen, P., Jensen, F.M., Middleton, C.R., and Blackmore, A. 1996. Assessment of the reliability of concrete slab bridges, 7th IFIP WG 7.5 Working Conference, Boulder, CO, 1-8.

Vu, K., Stewart, M.G., and Mullard, J. 2005. Corrosion-induced cracking: experimental data and predictive models, ACI Structural Journal, 102(5), 719-726.

Wilensky, U. 1999. NetLogo. Center for Connected Learning and Computer-Based Modeling, Northwestern University, Evanston, IL.

Wong, P.T.W., Lai, W.W.L., Sham, J.F.C., and Poon, C.-S. 2019. Hybrid non-destructive evaluation methods for characterizing chloride-induced corrosion in concrete, NDT and E International, 107, 202123.

Yehia, S., Abudayyeh, O., Nabulsi, S., and Abdelqader, I. 2007. Detection of common defects in concrete bridge decks using nondestructive evaluation techniques, Journal of Bridge Engineering, 12(2), 215-225.

University of Colorado Denver Inspection of Bridge Decks Utilizing Ground Penetrating Radar

FINAL REPORT

OCTOBER 1, 2018
BDI Project Number: 1804009-CO

Contents

On June 26th, 2018, BDI performed nondestructive testing of five (5) select bridge decks near Craig, CO to support the University of Colorado, Denver with research supporting the Colorado Department of Transportation. The objective of the testing was to identify technologies and best practices for inspection of bridge decks with asphalt overlays. Ground penetrating radar (GPR) was utilized on all five (5) decks at speeds from a crawling pace up to 50 mph in 10 mph increments. This corresponded with data collection rates in scans per foot accommodated by the GPR data acquisition system. Utilizing specialized data analysis software, BDI performed the analysis of the data to identify areas of potential degradation as well as those areas with precursors to degradation. Degradation precursors include chloride ingress, moisture, and loss of rebar cross section. Results include:
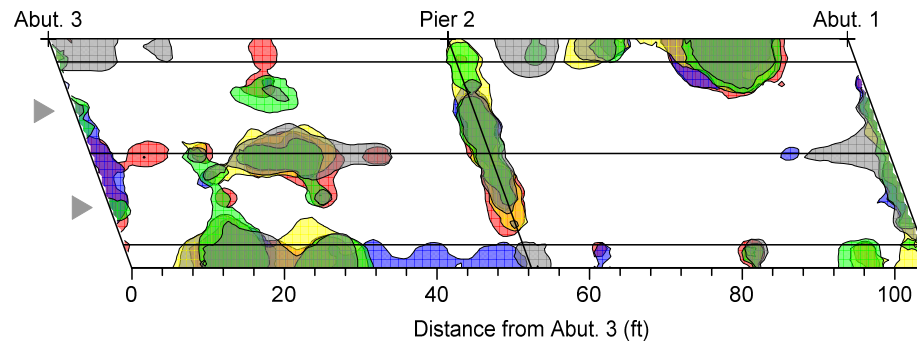
1. GPR analysis indicates that:
    a. Structure B-06-A, carrying US-40 westbound over Fortification Creek has average degradation of 14.14%, rebar depth of 5.2 in., and asphalt overlay of 2 in.
    b. Structure B-06-S, carrying US-40 eastbound over Fortification Creek has average degradation of 10.92%, rebar depth of 5.1 in., and asphalt overlay of 2.6 in.
    c. Structure B-06-V, carrying state highway 394 over the Yampa River has average degradation of 11.28%, rebar depth of 4.5 in., and asphalt overlay of 1.7 in.
    d. Structure C-07-A, carrying US-40 over the Yampa River has average degradation of 21.88%, rebar depth of 4.1 in., and asphalt overlay of 2 in.
    e. Structure C-08-A, carrying US-40 over the Shelton Ditch has average degradation of 8.84%, rebar depth of 4.9 in., and asphalt overlay of 2.6 in.
2. Varying speeds of data acquisition effected the results in the following manner:
    a. The maximum range and standard deviation of deterioration between data acquisition rates was 4.3% and 1.75%, respectively. Both of these values were found on Structure C-08-A. The minimum range and standard deviation were found on Structure B-06-A and were 1.8% and 0.67% respectively. With a maximum range of error of 4.3%.
3. The results indicate that reasonable spatial and quantitative correlation exists between the datasets acquired at all speeds tested.
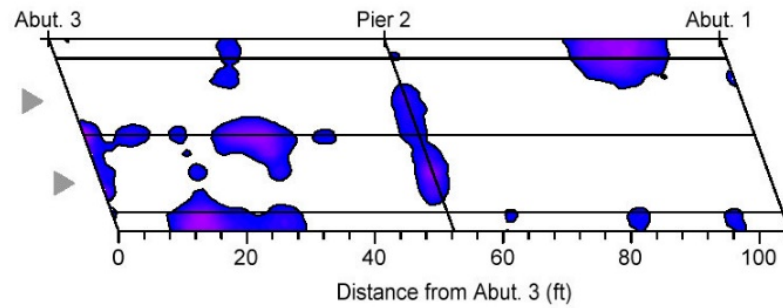
Introduction and Background

In May of 2018, the University of Colorado, Denver (UCD) contracted the services of BDI to perform a nondestructive evaluation (NDE) of five (5) select bridges in Colorado (Table 1). The objective of this project was to evaluate the condition of the five (5) bridge decks outlined in Table 1 using ground penetrating radar (GPR) at various data collection rates. The targeted speeds to be evaluated were from a crawling speed up to approximately 50 mph in 10 mph

increments. As GPR data collection is acquired based on scans per foot, BDI performed the maximum data collection rate at each corresponding speed (Table 2).

Table 1 – Bridges Identified for Study

Structure Number	Feature On	Feature Over
B-06-A	US-40 WB	Fortification Creek
B-06-S	US-40 EB	Fortification Creek
B-06-V	SH-394	Yampa River
C-07-A	US-40	Yampa River
C-08-A	US-40	Shelton Ditch

Table 2 – Data Collection Speeds

Scan Rates (scans/foot)	Max speeds (mph)	Target speeds for study (mph)
4	91.0	50
8	45.5	40
12	30.3	30
16	22.8	20
20*	18.2*	10* Crawling*

*As the maximum data collection speed for the equipment used was 20 scans per foot, the data collection resolution was the same at 10mph as it was at a crawling speed.

Testing and Analysis Activities

OVERVIEW

On June 26th, 2018, BDI performed data collection to satisfy the objectives of the project. The weather conditions were sunny, with temperatures in the upper-80s to mid-90s in degrees Fahrenheit. A total of five (5) datasets were collected for each bridge at target rates of crawling, 10mph, 20mph, 30mph, 40mph, and 50mph corresponding to the data collection rates in scans per foot presented in Table 2. The datasets were analyzed resulting in quantities and maps of structural concrete deterioration.

GROUND PENETRATING RADAR (GPR)

The GPR equipment included a dual 2-GHz air horn antenna system manufactured by GSSI, Inc. mounted to the rear of a BDI work vehicle (Figure 1). The antennas were approximately 15" above the pavement surface. The vehicle was equipped with an electronic distance-measuring instrument (DMI) mounted to the rear wheel, providing continuous distance data as the GPR data was collected. The data collection and recording were controlled by the GSSI SIR-20 GPR system operated from within the survey vehicle.

Figure 1 - GPR Survey Equipment

The GPR data was collected in a series of lines spaced at a maximum of 3 feet transversely across the width of each deck at targeted speeds ranging from crawling speed to approximately 50 mph in 10 mph increments. The survey included 9 to 11 lines of data for each deck; with each line representing a cross sectional slice of the deck at an offset.

Ground penetrating radar operates by transmitting short pulses of electromagnetic energy into an elastic material using an antenna attached to a survey vehicle. These pulses are reflected to the antenna with an arrival time and amplitude that is related to the location and nature of dielectric discontinuities in the material (air/asphalt or asphalt/concrete, reinforcing steel, etc.). The reflected energy is captured and may be displayed on an oscilloscope to form a series of pulses that are referred to as the radar signal. The signal contains a record of the properties and thicknesses of the layers within the structural member. By combining each sampled signal from the survey vehicle into a single image, features within the structural member can be identified.

The GPR analysis is carried out with GSSI's commercial software Radan 7, along with specialized software, using the following steps:

(1) Identification of the beginning and the end of the deck in each radar file, and check of the radar distance measurement against the known length and other features within the deck;
(2) Identification of features (top rebar, bottom of deck) that appear as dielectric discontinuities in the GPR data (see example data, Figures 2-3);
(3) Setup of the analysis for all the passes for a given deck, computation of concrete dielectric constant, rebar depth, and amplitude at the rebar-level.

Structural concrete deterioration can be inferred from changes in the dielectric properties and attenuation of the GPR signal in concrete. The dielectric constant is a measure of density, chloride and moisture content, and large variations in the dielectric constant can indicate concrete degradation.

A vacuum theoretically has a dielectric permittivity of 0 and would allow a complete transfer of these waves, and a perfect conductor would have an infinite dielectric permittivity and cause a perfect reflection of the waves. Air and steel act similarly to these cases, respectively, and thus, GPR can be used to identify steel reinforcement in structural concrete elements. Additionally, as the corrosion process occurs and iron oxide is formed, the dielectric properties of the material changes and the attenuation of the GPR signal is affected. The attenuation (loss of signal strength) of the radar signal, as measured from the top rebar reflection and/or the bottom of the deck, is used as a measure of concrete delamination. This is because contaminated and delaminated concrete will cause the GPR signal to dissipate and lose strength as it travels through the deck and reflects from the rebar and the bottom.

Interpreting this GPR data allows engineers and data scientists to precursors to degradation in structural concrete. These precursors, due to the nature of dielectric principles, include identification of high levels of chlorides, moisture, and possible cross section loss in structural concrete. The limitation to the technology is that it may present areas of degradation that does not correlate well to delaminations. This is because the results often identify areas of potential degradation rather than in place degradation. However, despite this limitation, GPR provides a strong tool for state DOTs to use to identify structures that have small quantities of delaminations but high levels of potential for degradation. This allows for prioritization of long-term planning for bridge maintenance and preservation.

Figure 2 provides a sample of GPR data with relatively consistent rebar reflections that appear to shift in depth between two adjacent spans and represents a section of bridge deck that does not exhibit any of the precursors for degradation mentioned above. Alternatively, Figure 3 provides a sample of GPR data presenting an area of relatively high amplitude rebar reflections, which are indicative of moisture and identifies two separate sections of bridge deck that could be considered to have a high probability of existing degradation or have precursors to degradation.
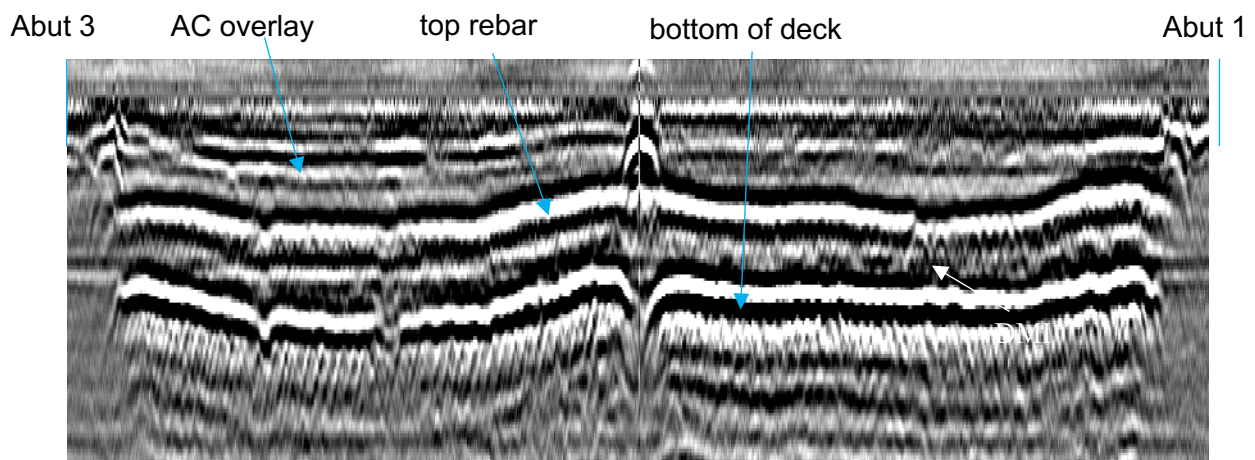
Figure 2 - Sample Single Scan GPR Data Presenting Limited Evidence of Deterioration on Structure B-06-A. This is a Sectional View of the Concrete Deck and is the Data from One Antenna.
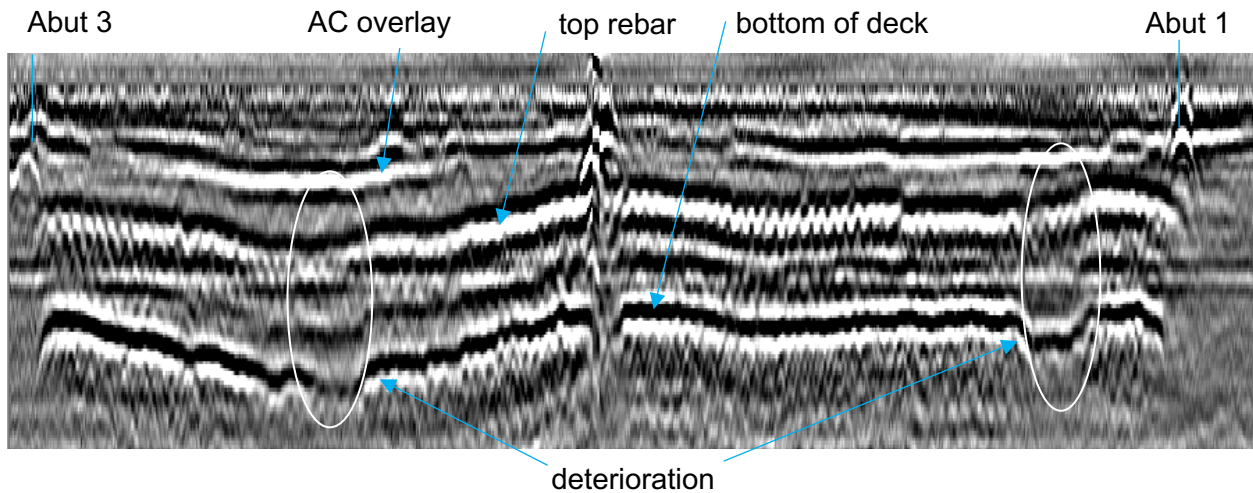
Figure 3 - Sample GPR Data Presenting Evidence of Deterioration on Structure B-06-A

Discussion of Results

The results of the deck condition evaluations include the quantities outlined in Table 3 and the condition maps provided in Appendix A. The deteriorated areas detected by GPR are shown in a blue to magenta color scale. The color scale indicates severity, which is related to the degree of the probability for precursors of degradation caused by chloride contamination and rebar corrosion. Table 2 presents the probable deterioration measured with GPR and Appendix A provides detailed GPR results. The maximum range and standard deviation of deterioration between data acquisition rates was 4.3% and 1.75%, respectively. Both of these values were found on Structure C-08-A. The minimum range and standard deviation were found on Structure B-06-A and were 1.8% and 0.67% respectively. With a maximum range of error of 4.3%, these results show reasonable spatial and quantitative correlation between the different datasets for each of the five bridge decks tested.

Table 3 – GPR Results

Structure Number	Total Square Footage (s.f)	Data Collection Rate (scans/foot)	Deterioration Detected by GPR (%)	Deterioration Detected by GPR (s.f.)	Average Deterioration (%)	Range (%)	Standard Deviation (%)	Average Rebar Depth (in.)	Average AC Overlay Thickness (in.)
B-06-A	2912	4	14.2	414	14.14	1.8	0.67	5.2	2
		8	13.8	402					
		12	14.3	416					
		16	13.3	387					
		20	15.1	440					
B-06-S	6720	4	9.8	659	10.92	2.8	1.15	5.1	2.6
		8	12.6	847					
		12	11.5	773					
		16	10	672					
		20	10.7	719					
B-06-V	11400	4	11.5	1311	11.28	2	0.74	4.5	1.7
		8	10.3	1174					
		12	11.4	1300					
		16	10.9	1243					
		20	12.3	1402					
C-07-A	8010	4	21.2	1698	21.88	2.8	1.14	4.1	2
		8	23.4	1874					
		12	20.6	1650					
		16	22.7	1818					
		20	21.5	1722					
C-08-A	684	4	10.9	75	8.84	4.3	1.75	4.9	2.6
		8	8.3	57					
		12	8.1	55					
		16	10.3	70					
		20	6.6	45					

Note(s) – Deterioration detected by GPR is the percentage and/or square footage of the bridge deck identified to have deterioration. For instance, B-06-A is approximately 2912 square feet, and an average of 14.14% was identified to be deteriorated with GPR testing and analysis. 14.14% of 2912 square feet is approximately 412 square feet. The range (%) is the range of deterioration detected by GPR (%) across all data collection rates for each bridge.

Conclusions and Recommendations

On June 26th, 2018, BDI performed nondestructive testing of five (5) select bridge decks near Craig, CO to support the University of Colorado, Denver with research supporting the Colorado Department of Transportation. The objective of the testing was to identify technologies and best practices for inspection of bridge decks with asphalt overlays. Ground penetrating radar (GPR) was utilized on all five (5) decks at speeds from a crawling pace up to 50 mph in 10 mph increments. This corresponded with data collection rates in scans per foot accommodated by the GPR data acquisition system. Utilizing specialized data analysis software, BDI performed the analysis of the data to identify areas of potential degradation as well as those areas with precursors to degradation. Degradation precursors include chloride ingress, moisture, and loss of rebar cross section. Results include:

1. GPR analysis indicates that:

a. Structure B-06-A, carrying US-40 westbound over Fortification Creek has average degradation of 14.14%, rebar depth of 5.2 in., and asphalt overlay of 2 in.

b. Structure B-06-S, carrying US-40 eastbound over Fortification Creek has average degradation of 10.92%, rebar depth of 5.1 in., and asphalt overlay of 2.6 in.

c. Structure B-06-V, carrying state highway 394 over the Yampa River has average degradation of 11.28%, rebar depth of 4.5 in., and asphalt overlay of 1.7 in.

d. Structure C-07-A, carrying US-40 over the Yampa River has average degradation of 21.88%, rebar depth of 4.1 in., and asphalt overlay of 2 in.

e. Structure C-08-A, carrying US-40 over the Shelton Ditch has average degradation of 8.84%, rebar depth of 4.9 in., and asphalt overlay of 2.6 in.

2. Varying speeds of data acquisition effected the results in the following manner:

a. The maximum range and standard deviation of deterioration between data acquisition rates was 4.3% and 1.75%, respectively. Both of these values were found on Structure C-08-A. The minimum range and standard deviation were found on Structure B-06-A and were 1.8% and 0.67% respectively. With a maximum range of error of 4.3%.

3. The results indicate that reasonable spatial and quantitative correlation exists between the datasets acquired at all speeds tested.

References

ASTM, "Standard Test Method for Evaluating Asphalt-Covered Concrete Bridge Decks Using Ground Penetrating Radar" Designation D 6087-08, ASTM International, West Conshohocken, PA, 2008.

SHRP C-101, "Condition Evaluation of Concrete Bridges Relative to Reinforcement Corrosion – Volume 3: Method of Evaluating the Condition of Asphalt-Covered Decks", Strategic Highway Research Program Report SHRP-S-325, Washington, DC, 1993.

APPENDIX A – GPR RESULTS

Abut. 3   Pier 2   Abut. 1

Distance from Abut. 3 (ft)

11

Abut. 3   Pier 2   Abut. 1
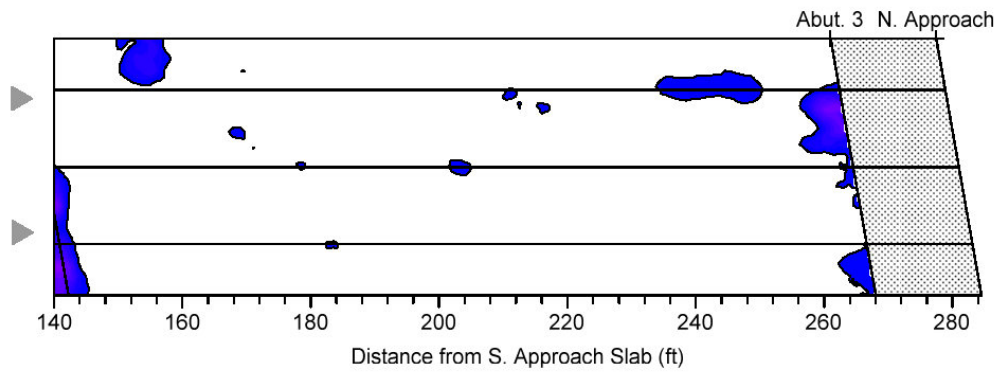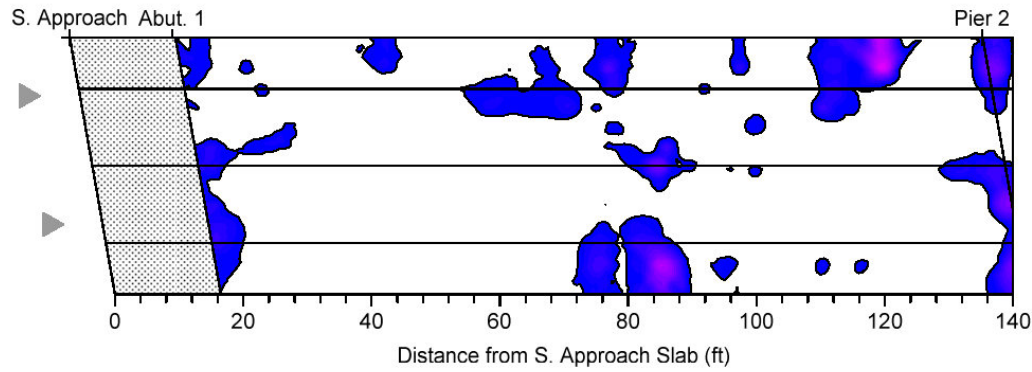
0   20   40   60   80   100
Distance from Abut. 3 (ft)

Concrete Condition Legend	Orientation	Quantity Summary		General Information
Deterioration Increasing severity --> Condition not detectable by GPR	N Direction of traffic	Deck	Conc. Deterioration (%)	14.2	Bridge ID: B-06-A (4 scans/ft) US 40 WB over Fortification Creek
			Conc. Deterioration (s.f)	446	Analyzed by: IN Reviewed by: SB Completed: 9/14/18
					Sheet 1 of 1

BDI
RAW DATA. REFINED RESULTS.

Abut. 3   Pier 2   Abut. 1

Distance from Abut. 3 (ft)

Concrete Condition Legend	Orientation	Quantity Summary		General Information
Deterioration Increasing severity --> ▦ Condition not detectable by GPR	N ▶ Direction of traffic	Deck	Conc. Deterioration (%)	13.8	Bridge ID: B-06-A (8 scans/ft) US 40 WB over Fortification Creek
			Conc. Deterioration (s.f)	432	Analyzed by: IN Reviewed by: SB Completed: 9/14/18
					Sheet 1 of 1

13

Concrete Condition Legend	Orientation	Quantity Summary			General Information
Deterioration Increasing severity --> ▨ Condition not detectable by GPR	N ▶ Direction of traffic	Deck	Conc. Deterioration (%)	14.3	Bridge ID: B-06-A (12 scans/ft) US 40 WB over Fortification Creek
			Conc. Deterioration (s.f)	449	Analyzed by: IN Reviewed by: SB Completed: 9/14/18
					Sheet 1 of 1

BDI
RAW DATA. REFINED RESULTS.

14

Concrete Condition Legend	Orientation	Quantity Summary		General Information
Deterioration Increasing severity --> ▨ Condition not detectable by GPR	N ▶ Direction of traffic	**Deck**	Conc. Deterioration (%)	13.3	Bridge ID: B-06-A (16 scans/ft) US 40 WB over Fortification Creek
			Conc. Deterioration (s.f)	417	Analyzed by: IN Reviewed by: SB Completed: 9/14/18
					Sheet 1 of 1

15

Concrete Condition Legend	Orientation	Quantity Summary		General Information
Deterioration Increasing severity --> [ ] Condition not detectable by GPR	N ▶ Direction of traffic	Deck	Conc. Deterioration (%)	15.1	Bridge ID: B-06-A (20 scans/ft) US 40 WB over Fortification Creek
			Conc. Deterioration (s.f)	472	Analyzed by: IN Reviewed by: SB Completed: 9/14/18
					Sheet 1 of 1

BDI — RAW DATA. REFINED RESULTS.

16

Abut. 1   Pier 2   Pier 3   Abut. 4

0   20   40   60   80   100   120

Distance from Abut. 1 (ft)

Concrete Deterioration Legend		Orientation		General Information	
4 spf/ 50mph	16 spf/ 20mph			Bridge ID: B-06-S US 40 EB over Fortification Creek	
8 spf/ 40mph	20 spf/ 10mph, Crawling			Analyzed by: IN Reviewed by: SB Completed: 9/7/18	
12 spf/ 30mph	Conditions not detectable	▶ Direction of traffic		Sheet 1 of 1	

BDI
RAW DATA. REFINED RESULTS.

17

Concrete Condition Legend	Orientation	Quantity Summary		General Information
Deterioration Increasing severity --> ▦ Condition not detectable by GPR	⟲ ▶ Direction of traffic	Deck	Conc. Deterioration (%) | 9.8 Conc. Deterioration (s.f) | 555	Bridge ID: B-06-S (4 scans/ft) US 40 EB over Fortification Creek Analyzed by: IN Reviewed by: SB Completed: 9/14/18 **Sheet 1 of 1**

| Abut. 1 | Pier 2 | Pier 3 | Abut. 4 |

Distance from Abut. 1 (ft)

Concrete Condition Legend	Orientation	Quantity Summary			General Information
Deterioration Increasing severity --> Condition not detectable by GPR	⤳ ▶ Direction of traffic	Deck	Conc. Deterioration (%)	12.6	Bridge ID: B-06-S (8 scans/ft) US 40 EB over Fortification Creek
			Conc. Deterioration (s.f)	717	Analyzed by: IN Reviewed by: SB Completed: 9/14/18
					Sheet 1 of 1

BDI
RAW DATA. REFINED RESULTS.

19
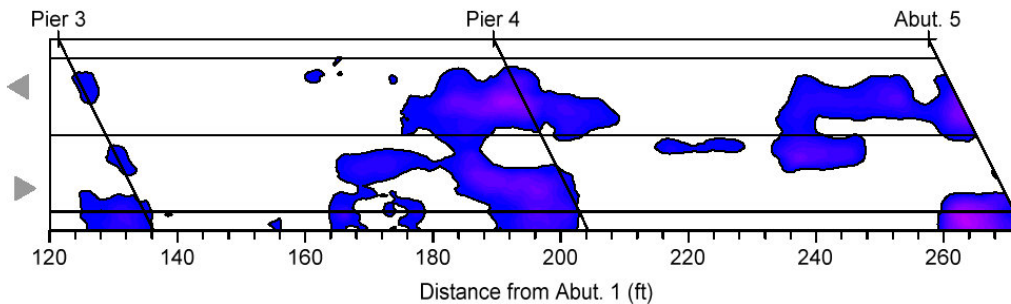
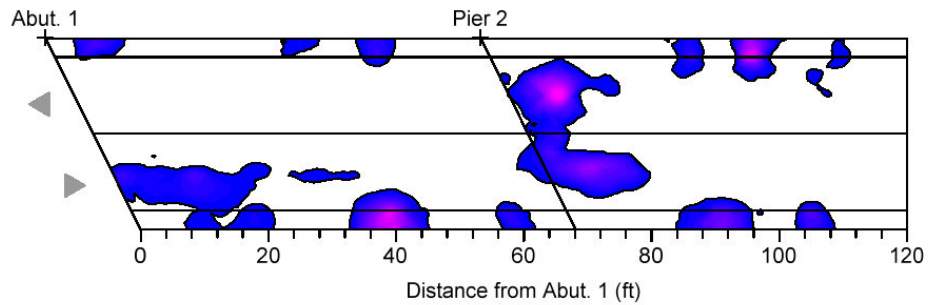| Concrete Condition Legend	Orientation	Quantity Summary			General Information
Deterioration Increasing severity --> ▨ Condition not detectable by GPR	⇗ ▶ Direction of traffic	Deck	Conc. Deterioration (%)	11.5	Bridge ID: B-06-S (12 scans/ft) US 40 EB over Fortification Creek
			Conc. Deterioration (s.f)	654	Analyzed by: IN Reviewed by: SB Completed: 9/14/18
					Sheet 1 of 1

20

Concrete Condition Legend	Orientation	Quantity Summary			General Information
Deterioration Increasing severity --> ▨ Condition not detectable by GPR	⇄➡ ▶ Direction of traffic	Deck	Conc. Deterioration (%)	10.0	Bridge ID: B-06-S (16 scans/ft) US 40 EB over Fortification Creek
			Conc. Deterioration (s.f)	572	Analyzed by: IN Reviewed by: SB Completed: 9/14/18
					Sheet 1 of 1

21

Concrete Condition Legend	Orientation	Quantity Summary		General Information	
Deterioration		Deck	Conc. Deterioration (%)	10.7	Bridge ID: B-06-S (20 scans/ft) US 40 EB over Fortification Creek
Increasing severity -->			Conc. Deterioration (s.f)	609	Analyzed by: IN Reviewed by: SB Completed: 9/14/18
Condition not detectable by GPR	▶ Direction of traffic				Sheet 1 of 1

Concrete Deterioration Legend		Orientation		General Information
4 spf/ 50mph	16 spf/ 20mph			Bridge ID: B-06-V SH 394 over Yampa River
8 spf/ 40mph	20 spf/ 10mph, Crawling			Analyzed by: IN Reviewed by: SB Completed: 9/7/18
12 spf/ 30mph	Conditions not detectable	Direction of traffic		**Sheet 1 of 1**

S. Approach Abut. 1   Pier 2

Distance from S. Approach Slab (ft)

Abut. 3 N. Approach

Distance from S. Approach Slab (ft)

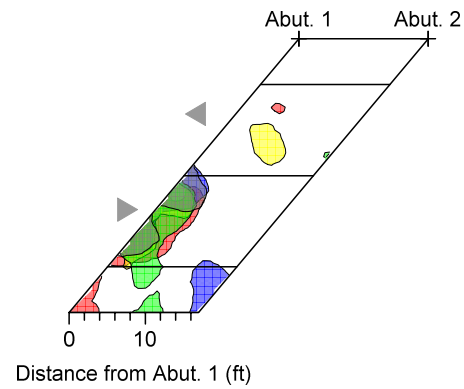| Concrete Condition Legend	Orientation	Quantity Summary			General Information
Deterioration Increasing severity --> Approach Slab	⇄ ➤ ▶ Direction of traffic	Deck	Conc. Deterioration (%)	11.5	Bridge ID: B-06-V (4 scans/ft) SH 394 over Yampa River
			Conc. Deterioration (s.f)	1158	Analyzed by: IN Reviewed by: SB Completed: 9/14/18
					Sheet 1 of 1

BDI
RAW DATA. REFINED RESULTS.

S. Approach Abut. 1
Pier 2

Distance from S. Approach Slab (ft)

Abut. 3 N. Approach

Distance from S. Approach Slab (ft)

Concrete Condition Legend	Orientation	Quantity Summary		General Information
Deterioration Increasing severity --> ▨ Approach Slab	⇄ ▶ Direction of traffic	Deck	Conc. Deterioration (%)	10.3	Bridge ID: B-06-V (8 scans/ft) SH 394 over Yampa River
			Conc. Deterioration (s.f)	1030	Analyzed by: IN Reviewed by: SB Completed: 9/14/18
					Sheet 1 of 1

BDI
RAW DATA. REFINED RESULTS.

25

S. Approach Abut. 1   Pier 2

Distance from S. Approach Slab (ft)

Abut. 3 N. Approach

Distance from S. Approach Slab (ft)

Concrete Condition Legend	Orientation	Quantity Summary		General Information
Deterioration Increasing severity --> Approach Slab	Direction of traffic	Deck	Conc. Deterioration (%)	11.4	Bridge ID: B-06-V (12 scans/ft) SH 394 over Yampa River
			Conc. Deterioration (s.f)	1150	Analyzed by: IN Reviewed by: SB Completed: 9/14/18
					Sheet 1 of 1

BDI
RAW DATA. REFINED RESULTS.

26

S. Approach Abut. 1

Pier 2

Distance from S. Approach Slab (ft)

Abut. 3 N. Approach

Distance from S. Approach Slab (ft)

Concrete Condition Legend	Orientation	Quantity Summary		General Information
Deterioration Increasing severity -->	⇉	Deck	Conc. Deterioration (%)	10.9	Bridge ID: B-06-V (16 scans/ft) SH 394 over Yampa River
			Conc. Deterioration (s.f)	1096	Analyzed by: IN Reviewed by: SB Completed: 9/14/18
▨ Approach Slab	▶ Direction of traffic				Sheet 1 of 1

BDI
RAW DATA. REFINED RESULTS.

27

S. Approach Abut. 1   Pier 2

Distance from S. Approach Slab (ft)

Abut. 3 N. Approach

Distance from S. Approach Slab (ft)

Concrete Condition Legend	Orientation	Quantity Summary			General Information
Deterioration Increasing severity -->		Deck	Conc. Deterioration (%)	12.3	Bridge ID: B-06-V (20 scans/ft) SH 394 over Yampa River
			Conc. Deterioration (s.f)	1238	Analyzed by: IN Reviewed by: SB Completed: 9/14/18
Approach Slab	Direction of traffic				Sheet 1 of 1

| Abut. 1 | Pier 2 | Pier 3 | Pier 4 | Abut. 5 |

Distance from Abut. 1 (ft)

Concrete Deterioration Legend		**Orientation**		**General Information**	
🔴 4 spf/ 50mph	🟢 16 spf/ 20mph	**N**		Bridge ID: C-07-A US 40 over Yampa River	
🔵 8 spf/ 40mph	⬜ 20 spf/ 10mph, Crawling			Analyzed by: IN Reviewed by: SB Completed: 9/7/18	
🟡 12 spf/ 30mph		▶ Direction of traffic		**Sheet 1 of 1**	

BDI
RAW DATA. REFINED RESULTS.

29

Concrete Condition Legend	Orientation	Quantity Summary			General Information
Deterioration Increasing severity --> Condition not detectable by GPR	N ▶ Direction of traffic	Deck	Conc. Deterioration (%)	21.2	Bridge ID: C-07-A (4 scans/ft) US 40 over Yampa River
			Conc. Deterioration (s.f)	1732	Analyzed by: IN Reviewed by: SB Completed: 9/14/18
					Sheet 1 of 1

Abut. 1   Pier 2

Distance from Abut. 1 (ft)

Pier 3   Pier 4   Abut. 5

Distance from Abut. 1 (ft)

Concrete Condition Legend	Orientation	Quantity Summary			General Information
Deterioration Increasing severity --> Condition not detectable by GPR	N ▶ Direction of traffic	Deck	Conc. Deterioration (%)	23.4	Bridge ID: C-07-A (8 scans/ft) US 40 over Yampa River
			Conc. Deterioration (s.f)	1908	Analyzed by: IN Reviewed by: SB Completed: 9/14/18
					Sheet 1 of 1

BDI
RAW DATA. REFINED RESULTS.

31

Abut. 1   Pier 2

0   20   40   60   80   100   120

Distance from Abut. 1 (ft)

Pier 3   Pier 4   Abut. 5

120   140   160   180   200   220   240   260

Distance from Abut. 1 (ft)

Concrete Condition Legend	Orientation	Quantity Summary			General Information
Deterioration Increasing severity --> Condition not detectable by GPR	N ▶ Direction of traffic	Deck	Conc. Deterioration (%)	20.6	Bridge ID: C-07-A (12 scans/ft) US 40 over Yampa River
			Conc. Deterioration (s.f)	1685	Analyzed by: IN Reviewed by: SB Completed: 9/14/18
					Sheet 1 of 1

BDI
RAW DATA. REFINED RESULTS.

32

Abut. 1   Pier 2

Distance from Abut. 1 (ft)

Pier 3   Pier 4   Abut. 5

Distance from Abut. 1 (ft)

Concrete Condition Legend	Orientation	Quantity Summary		General Information
Deterioration Increasing severity --> Condition not detectable by GPR	N ▶ Direction of traffic	Deck	Conc. Deterioration (%)	22.7	Bridge ID: C-07-A (16 scans/ft) US 40 over Yampa River
			Conc. Deterioration (s.f)	1853	Analyzed by: IN Reviewed by: SB Completed: 9/14/18
					Sheet 1 of 1

33

Concrete Condition Legend	Orientation		Quantity Summary		General Information	
Deterioration Increasing severity --> [░] Condition not detectable by GPR	[North arrow symbol] [▶] Direction of traffic	Deck	Conc. Deterioration (%)	21.5	Bridge ID: C-07-A (20 scans/ft) US 40 over Yampa River	
			Conc. Deterioration (s.f)	1756	Analyzed by: IN Reviewed by: SB Completed: 9/14/18	
					Sheet 1 of 1	

Abut. 1   Abut. 2

0   10

Distance from Abut. 1 (ft)

Concrete Deterioration Legend		Orientation		General Information
4 spf/ 50mph	16 spf/ 20mph			Bridge ID: C-08-A US 40 over Shelton Ditch
8 spf/ 40mph	20 spf/ 10mph, Crawling	N		Analyzed by: IN Reviewed by: SB Completed: 9/7/18
12 spf/ 30mph		Direction of traffic		**Sheet 1 of 1**

Abut. 1   Abut. 2

Distance from Abut. 1 (ft)

Concrete Condition Legend	Orientation	Quantity Summary		General Information
Deterioration Increasing severity -->		**Deck** Conc. Deterioration (%)	10.9	Bridge ID: C-08-A (4 scans/ft) US 40 over Shelton Ditch
		Conc. Deterioration (s.f)	63	Analyzed by: IN Reviewed by: SB Completed: 9/14/18
Condition not detectable by GPR	▶ Direction of traffic			**Sheet 1 of 1**

Distance from Abut. 1 (ft)

Concrete Condition Legend	Orientation	Quantity Summary		General Information
Deterioration Increasing severity --> ▨ Condition not detectable by GPR	↗N ▶ Direction of traffic	Deck	Conc. Deterioration (%)	8.3	Bridge ID: C-08-A (8 scans/ft) US 40 over Shelton Ditch
			Conc. Deterioration (s.f)	48	Analyzed by: IN Reviewed by: SB Completed: 9/14/18
					Sheet 1 of 1

Abut. 1   Abut. 2

0   10
Distance from Abut. 1 (ft)

Concrete Condition Legend	Orientation	Quantity Summary		General Information
Deterioration Increasing severity --> Condition not detectable by GPR	⬈N ▶ Direction of traffic	Deck	Conc. Deterioration (%)	8.1	Bridge ID: C-08-A (12 scans/ft) US 40 over Shelton Ditch
			Conc. Deterioration (s.f)	47	Analyzed by: IN Reviewed by: SB Completed: 9/14/18
					Sheet 1 of 1

BDI
RAW DATA. REFINED RESULTS.

38

Abut. 1   Abut. 2

0   10
Distance from Abut. 1 (ft)

Concrete Condition Legend	Orientation	Quantity Summary		General Information
Deterioration Increasing severity --> Condition not detectable by GPR	Direction of traffic	Deck	Conc. Deterioration (%)	10.3	Bridge ID: C-08-A (16 scans/ft) US 40 over Shelton Ditch
			Conc. Deterioration (s.f)	59	Analyzed by: IN Reviewed by: SB Completed: 9/14/18
					Sheet 1 of 1

Abut. 1   Abut. 2

0   10

Distance from Abut. 1 (ft)

Concrete Condition Legend	Orientation	Quantity Summary			General Information
Deterioration Increasing severity --> Condition not detectable by GPR	◢N ▶ Direction of traffic	Deck	Conc. Deterioration (%)	6.6	Bridge ID: C-08-A (20 scans/ft) US 40 over Shelton Ditch
			Conc. Deterioration (s.f)	38	Analyzed by: IN Reviewed by: SB Completed: 9/14/18
					Sheet 1 of 1

BDI
RAW DATA. REFINED RESULTS.

40